Review

Freeform 3D printing of vascularized tissues: Challenges and strategies

Journal of Tissue Engineering
Volume 12: 1–34

DOI: 10.1177/20417314211057236
journals.sagepub.com/home/tej
SAGE

Hyun Lee[1,2*], Tae-Sik Jang[3*], Ginam Han[1,2], Hae-Won Kim[4,5,6,7,8] and Hyun-Do Jung[1,2]

Abstract

In recent years, freeform three-dimensional (3D) printing has led to significant advances in the fabrication of artificial tissues with vascularized structures. This technique utilizes a supporting matrix that holds the extruded printing ink and ensures shape maintenance of the printed 3D constructs within the prescribed spatial precision. Since the printing nozzle can be translated omnidirectionally within the supporting matrix, freeform 3D printing is potentially applicable for the fabrication of complex 3D objects, incorporating curved, and irregular shaped vascular networks. To optimize freeform 3D printing quality and performance, the rheological properties of the printing ink and supporting matrix, and the material matching between them are of paramount importance. In this review, we shall compare conventional 3D printing and freeform 3D printing technologies for the fabrication of vascular constructs, and critically discuss their working principles and their advantages and disadvantages. We also provide the detailed material information of emerging printing inks and supporting matrices in recent freeform 3D printing studies. The accompanying challenges are further discussed, aiming to guide freeform 3D printing by the effective design and selection of the most appropriate materials/processes for the development of full-scale functional vascularized artificial tissues.

Keywords

Additive manufacturing, freeform 3D printing, vascularized structures, artificial tissues, tissue engineering

Date received: 21 August 2021; accepted: 17 October 2021

[1]Department of Biomedical and Chemical Engineering (BMCE), The Catholic University of Korea, Bucheon, Republic of Korea
[2]Department of Biotechnology, The Catholic University of Korea, Bucheon-si, Gyeonggi-do, Republic of Korea
[3]Department of Materials Science and Engineering, Chosun University, Gwangju, Republic of Korea
[4]Institute of Tissue Regeneration Engineering (ITREN), Dankook University, Cheonan, Chungcheongnam-do, Republic of Korea
[5]Department of Biomaterials Science, College of Dentistry, Dankook University, Cheonan, Chungcheongnam-do, Republic of Korea
[6]Department of Nanobiomedical Science & BK21 PLUS NBM Global Research Center for Regenerative Medicine, Dankook University, Cheonan, Chungcheongnam-do, Republic of Korea
[7]Cell & Matter Institute, Dankook University, Cheonan, Chungcheongnam-do, Republic of Korea
[8]Department of Regenerative Dental Medicine, College of Dentistry, Dankook University, Cheonan, Chungcheongnam-do, Republic of Korea

*The authors have equally contributed to this work.

Corresponding authors:
Hae-Won Kim, Institute of Tissue Regeneration Engineering (ITREN), Dankook University, 119 Dandae-ro, Cheonan, Chungcheongnam-do 31116, Republic of Korea.
Email: kimhw@dku.edu

Hyun-Do Jung, Department of Biotechnology, The Catholic University of Korea, 43 Jibong-ro, Wonmi-gu, Bucheon-si, Gyeonggi-do 14662, Republic of Korea.
Email: hdjung@catholic.ac.kr

Introduction

Cardiovascular diseases including coronary artery diseases, strokes, and venous thromboembolism have been acknowledged as primary causes of death.[1,2] Most of the mentioned diseases are mainly caused by aging and deposition of cholesterol on the wall of vessels which are closely related to factors narrowing blood vessels. Since blood vessels are the pathway to deliver nutrients and cells to every parts of the human body, narrowed blood vessels should be expanded not to induce further complications. There have been numerous approaches to manage cardiovascular diseases. Vascular bypass using auto-grafts or artificial vascular grafts or vascular stents with the aid of balloons and catheter have been widely utilized.[3–5] In particular, artificial vascular grafts and vascular stents have been extensively researched since there are limitations in auto-graft sources. Artificial grafts consisting of polymeric matrices such as poly(ε-caprolactone) (PCL), expanded form of PTFE (ePTFE), and polyurethane (PU), exhibited successful results in vascular applications.[6–8] In addition, vascular stents made from synthetic polymers and metallic materials with various surface modifications showed their effectiveness by in vitro and in vivo examinations in recent articles.[6,9–14] However, there have been needs for creating artificial vascular grafts with customized structures to meet versatile structure of each patients and each surgical sites.

Over the last few years, additive manufacturing (AM), or 3D printing, has proven its capability to fabricate three-dimensional (3D) objects with good precision and resolution and has gone through an enormous transformation in biomedical applications.(*)[15–19] In particular, computer-aided designs and the layer-by-layer manufacturing steps of 3D printing make it possible to fabricate customized 3D constructs for patients, surgical planning prototypes, and living tissues.[20–24] In this way, computational science, material science, and biology are integrated to selectively deposit biologically compatible materials, living cells, drugs, and biomolecules, and fabricate complex architectures that resemble the shape and function of human tissues and organs.[25,26] However, the major challenge is to precisely replicate the vascularized multiscale architecture of human tissues with delicate biological materials like hydrogels, cells, and extracellular matrices (ECMs), typically in a layer-by-layer fashion.[26,27] The structure of blood vessels mainly consist of three different layers including adventitia, media, and intima as illustrated in Figure 1(a). The main role of adventitia is to provide structural integrity to the whole vessel which includes collagen, ECMs, and fibroblasts.[28,29] On the other hand, media which is composed of smooth muscle cells (SMCs) and pericytes is the thickest layer among the three layers, and it renders load bearing capability.[30] Intima is an innermost layer of blood vessels which adjusts vascular tones and it is comprised of endothelial cells (ECs).[30] Based on function and structure, blood vessels can be classified into arteries, capillaries, and veins (Figure 1(a)). Because of highly precise and complicated structure and composition of the layers in vessels, fabrication of artificial vasculature has been challenging. Despite the difficulties, incorporating microvascular networks in artificial tissues is functionally the most important factor for successful long-term tissue replacement because blood vessels are essential for the transportation of nutrients and oxygen to cells.[31] In addition, as the mechanical properties of the printed materials need to match those of the human tissues, the 3D printing materials with limited mechanical strength have difficulty in retaining the 3D structures and shapes during printing and curing without additional support in soft tissue applications.[25,27,32]

In recent years, an emerging 3D printing strategy called freeform 3D printing, has attracted the attention of researchers due to its unique printing characteristics. Freeform 3D printing refers to the new AM process that involves two main components of printing materials and supporting matrices and directly builds 3D curves instead of 2D layers without any additional supporting structures.[19,25] This technique allows the deposition of materials in any spatial direction using a sacrificial supporting matrix, and ensures shape maintenance of the printed 3D constructs with the desired spatial control.[19,25,27] As human tissues are generally curved and irregularly shaped, the freeform 3D printing system is potentially applicable for the fabrication of human tissue replacements compared to conventional 3D printing systems with flat and planar printing sequences.[33] In addition, during the freeform 3D printing process, the supporting matrix can prevent the collapse of soft and weak printed 3D constructs, and provides additional time for curing or crosslinking of the printed materials, which ensures the mechanically relevant strength and structural integrity even after removing the supporting matrix.[19,25,27] Since the introduction of the freeform 3D printing system by Wu et al.,[34] there have been many attempts to fabricate complex 3D objects that are generally difficult to fabricate using conventional 3D printing. Furthermore, freeform 3D printing has proven its ability by successfully fabricating various 3D structures, such as hemispherical shells, porous scaffolds, and hierarchical hollow structures with large overhangs.[25,27,34]

In the freeform 3D printing system, the supporting matrix requires viscoplasticity with a yield stress; the supporting matrix should behave like a liquid when the applied stress is above the yield stress and as a solid when the applied stress is below the yield stress.[25,35] This solid–liquid transition of the supporting matrix allows free movement of the printing nozzle within the supporting matrix without mechanical resistance, while it holds the printed materials stably, preventing disruption of pre-printed structures throughout the printing process. Based on this

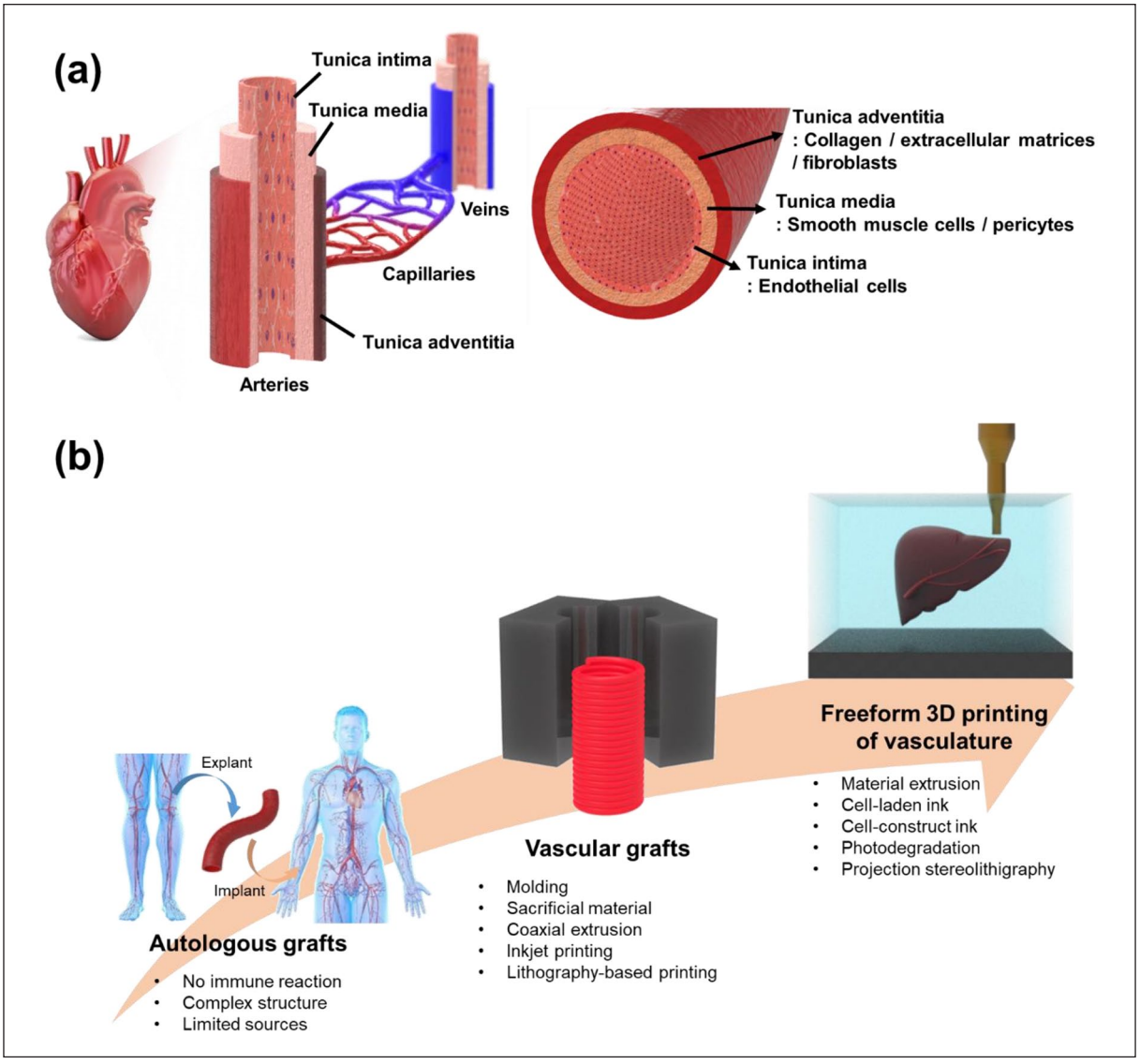

Figure 1. (a) Diagrammatic demonstration of vascular system and regional classification of blood vessel and (b) schematic illustration showing the trends in fabrication of tissues with vascularized structures.

property, significant progress has been made in the development of positive and negative freeform 3D printing systems to fabricate vascular network structures.[25] The positive freeform 3D printing system directly produces hollow tubes or interconnected channel structures after the printed material is cured, whereas in the negative freeform 3D printing systems, sacrificial inks are removed after printing the desired vascular network structures, and the supporting matrix becomes the final artificial tissue.[25,36–39] Herein, we provide the first overview of recent advances in freeform 3D printing to fabricate artificial tissues with vascular structures and their applications in the field of tissue engineering. We shall compare conventional 3D printing and freeform 3D printing technologies and discuss their working principles for developing vascular constructs (Figure 1(b)). Additionally, several emerging printing inks and supporting matrices for freeform 3D printing and their accompanying challenges are discussed in parallel.

Conventional strategy for developing vascular constructs

Vascular constructs have attracted increasing interest for replacing and bypassing diseased or damaged blood vessels caused by cardiovascular diseases (CVDs). Such constructs are critical for supplying nutrients and oxygen, as well as removing the waste of living cells in artificial organs. Various methods have been developed to construct mammalian vascular systems, which consist of a 3D network ranging from larger arteries (0.4–8 mm diameter) to microvessels and capillaries (10–50 μm diameter). The conventional strategies for fabrication of vascular

constructs can be categorized into (i) molding strategy, (ii) sacrificial material strategy, (iii) coaxial extrusion strategy, (iv) inkjet printing strategy, and (v) lithography-based printing strategy. These categorizations will help in the process of selecting appropriate techniques for achieving the desired vascular constructs. Every strategy has an innovative combination of entirely different approaches and materials that achieve not only structural diversity (i.e. vascular diameter) for adapting numerous vascular applications, but also a plurality of functions such as mechanical properties, hemocompatibility, and degradation controllability. A combination of multiple techniques would catalyze the intense research activities of artificial tissues with vascularized structures for various tissue-engineering applications. Figure 2 and Table 1 provide a summary of the conventional strategies.

Molding strategy

The molding technique, also known as the casting technique, is a versatile method that has been applied extensively to model complex architectures of vascular constructs that closely mimic real blood vessels. It is a cost-effective and easy-to-implement method in which mechanically and chemically isotropic constructs can be obtained. Moreover, with the aid of developed scanning and 3D printing techniques, individually customized vascular tissues could be fabricated for patients who have suffered different types of loss or damage.

Gupta et al.[40] studied small-diameter vascular constructs with bi-layers based on bioresorbable silk materials using custom-designed 3D printed molds consisting of a base and cap. Prepared silk fibroin (SF) hydrogel was poured into the space between the central rod and tube followed by freezing at −20°C. Following the extraction of the central rod, the frozen tubular SF was lyophilized. Finally, the porous tubular silk constructs were coated with a combination of polycaprolactone (PCL) and silk through an electrospinning process. The fabricated vascular constructs had a porous inner layer, with ideally sized (~40 μm) pores and ~90% porosity, and a relatively dense outer layer that conferred mechanical resilience in both longitudinal and circumferential directions. Stromal vascular fraction cells dynamically cultured on the silk constructs showed good viability and metabolic activity. In vivo rat aortic implantation of the silk constructs displayed superior animal survival and graft patency. Moreover, histological analysis revealed host cell infiltration, neo-tissue formation without aneurysm formation, as well as vascular construct remodeling in terms of the ECM, demonstrating the potential of a new and facile molding-based technique to develop biodegradable vascular constructs.

However, native vascular constructs have a complex structure that includes side branches, thus a different mold strategy is needed to fabricate the complex vascular structure. Wang et al.[41] fabricated an ice mold using a 3D printing technique for freestanding hierarchical vascular constructs. The procedure of casting ice molds for vascular constructs was composed of three sequential stages: (i) modeling and casting a negative polydimethylsiloxane (PDMS) mold using a 3D printed positive polylactide mold, (ii) freezing water in the PDMS mold and then demolding it, and (iii) dipping the positive ice mold in numerous vascular construct materials and stabilizing it to form a tubular structure. The structural properties, such as diameter and wall thickness, were tailored by the 3D printing and coating conditions. The fabricated tropoelastin vessels with PCL showed similar burst pressure and tensile property values (ultimate tensile strength (UTS) and Young's modulus) to the human saphenous vein. The fabricated tropoelastin vascular walls were suitable for the growth and proliferation of human umbilical vein endothelial cells (HUVECs). In the same study, complex shaped vascular constructs were fabricated by direct 3D printing of ice. The researchers maintained the 3D printing conditions at a subzero environment such that liquid water from the print head could be extruded as solid ice on a bedplate. With 3D printing of ice, freestanding positive complex vascular shaped molds could be acquired, and perfectly perfusable hierarchical vascular constructs, such as a bifurcation, network, and loop design, were formed by the same dip coating process.

In contrast, the possibility of using a rotary mandrel mold for the fabrication of vascular structures was verified using electrospinning and modified 3D printing techniques. The electrospinning technique has been widely used for the production of polymeric fiber structures with controllable fiber diameter and pattern. Furthermore, one of the attractive features of electrospinning for vascular applications is the ease of manufacturing tubular shapes because electrospun fibers are collected by a rotated cylindrical mandrel called a collector. Inoguchi et al.[42] reported that "mechano-active" artificial vascular grafts with small diameters could be fabricated by electrospinning. Using a 3 mm diameter positive mold similar to small-diameter blood vessels, a tubular elastomeric poly(L-lactide-co-e-caprolactone) (PLCL) construct was directly obtained. The electrospun elastomeric PLCL construct pulsated synchronously in a custom-designed arterial circulatory system. Bilayered nanofibrous vascular constructs with improved mechanical properties and bioactivity were also produced by the electrospinning technique.[6] The electrospun structure was composed of a randomly oriented PCL/silica outer layer for enhanced mechanical properties and fibroblast affinity, and a longitudinally aligned PLC/collagen inner layer for promoted endothelial cell adherence and rapid migration. The fabricated bilayer vascular constructs showed higher tensile properties in terms of the longitudinal and circumferential directions, than those of the human coronary artery. Released Si ions from the outer PCL/silica

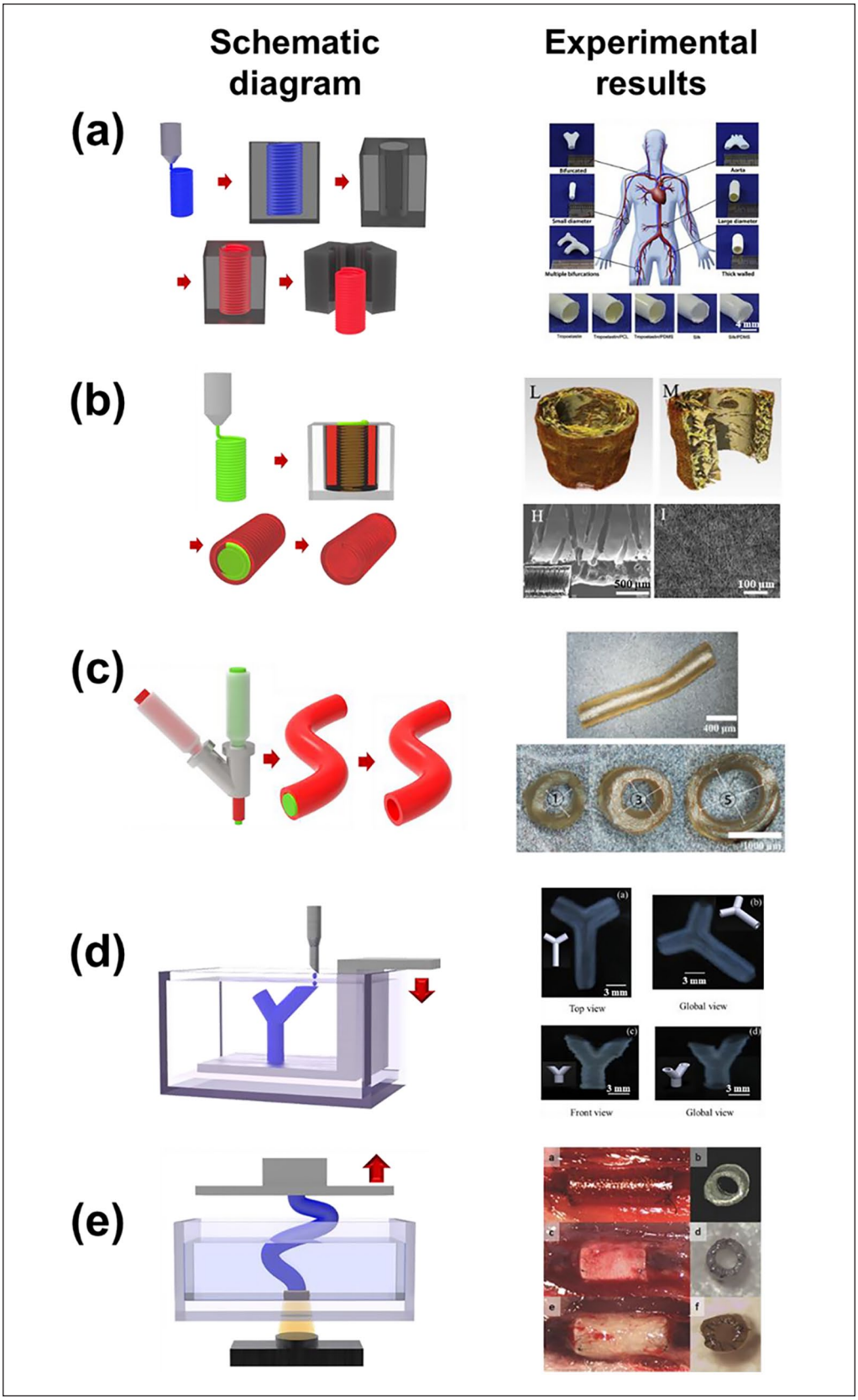

Figure 2. Schematic diagram and representative experimental results of (a) molding strategy (adapted with permission from Wang et al.[41]), (b) sacrificial material strategy (adapted with permission from Wu et al.[46]), (c) coaxial extrusion strategy (adapted with permission from Zeng et al.[52]), (d) inkjet printing strategy (adapted with permission from Christensen et al.[59]), and (e) lithography-based printing strategy (adapted with permission from Melchiorri et al.[60]).

Table 1. Overview of conventional strategy for developing vascular constructs.

3D printing approach	Materials	Vascular construct size	Mechanical properties	Significance	References
Custom-designing 3D printed base and cap molds	Silk + PCL	Diameter: 918 μm Thickness: 718 μm Length: 3 cm	UTS: 0.34–0.36 MPa Modulus: 0.21–0.31 MPa Suture retention force: 0.38–0.46 N Suture retention tension: 520–620 N/m Dynamic compliance: 1%–2%/100 mmHg Burst pressure: 798–827 mmHg	Bi-layered silk tissue-engineered vascular graft with optimal porosity, mechanical resilient, and biodegradability	Gupta et al.[40]
Casting ice molds using 3D printed PLA molds	Tropoelastin + PCL	Diameter: 6–8 mm Thickness: 261–900 μm	UTS: 0.9–1.2 MPa Modulus: 5–10 MPa Suture retention force: 210–280 N Burst pressure: 1128 mmHg	Fabrication of freestanding hierarchical vascular structures with variable lumen dimensions	Wang et al.[41]
Electrospinning with single layer	PLCL	Diameter: 2.3–2.5 mm Thickness: 50–340 μm	—	"Mechano-active" small-diameter artificial vascular graft	Inoguchi et al.[42]
Electrospinning with bi-layer	PCL + silica + collagen	Diameter: 3 mm Thickness: 500 μm Length: 4 mm	UTS: 1.2–3.3 MPa Modulus: 4–21 MPa Elongation at break: 60%–150% Suture retention stress: 2.7 MPa	Novel design for a small-diameter PCL vascular graft with a functional, bilayered nanofibrous structures	Park et al.[7]
3D printing system with XθZ-axis	Alginate + gelatin	Diameter: 3–6.9 mm Thickness: 0.5–3 mm	—	Novel 3D printing system using a rotary forming device to fabricate vessel-like structures	Liu et al.[43]
3D printing + electrospinning	PLLA + Hep + PCL	Diameter: 5 mm Thickness: 0.3 mm Length: 6 cm	UTS: 1.58 MPa Modulus: 0.21–0.31 MPa Elongation at break: 178% Suture retention force: 1.31 N Suture retention tension: 4.85 N/m Static compliance: 9.72%/100mmHg Burst pressure: 0.3 MPa	Combined both electrospinning and 3D printing systems for vascular construct application	Centola et al.[44]
3D printing + electrospinning	PCL + PDA + VEGF	Diameter: 3 mm Thickness: 0.3 mm Length: 6 cm	—	Bilayered structure with inner aligned nanofibrous layer and stent-like outer layer	Lee et al.[45]
Melt-spinning sacrificial sugar microfibers + electrospinning	PLCL	Diameter: 2 mm Thickness: 0.6 mm Length: 2 cm	UTS: 5.2–7.3 MPa Modulus: 13.4–15.7 MPa Elongation at break: 175%–184% Burst pressure: 1787–2181 mmHg	Bi-layered vascular constructs with a circumferentially aligned microchannels structure	Wu et al.[46]
3D printing PVA sacrificial core + TPU dip coating	TPU	Diameter: 5 mm Thickness: 0.4 mm Length: 5 cm	Elongation at break: 178% Suture retention force: 2.67 N Compliance: 2.03%/100 mmHg Burst pressure: 0.3 MPa, 2250 mmHg	Triple-layered constructs designed to mimic native blood vessels with each layer contributing its unique porosity to the porous structure	Wang et al.[47]
3D printing PVA sacrificial core + TPU/NaCl dip coating	TPU	Diameter: 5, 10, 15 mm Length: 5 cm	UTS: 15 MPa Modulus: 19 MPa Elongation at break: 456%	Customized porous TPU vascular constructs by dip-coating procedure with NaCl-suspended TPU	Sohn et al.[48]
3D printing PVA sacrificial core + PDMS dip coating	PDMS	Diameter: 0.3–0.8 mm Thickness: 0.3–0.9 mm	UTS: 0.6 MPa YS: 0.5 MPa Modulus: 1.6 MPa Elongation at break: 57.2%	Artificial PDMS blood vessel in a right-hand surgical replica	Park et al.[49]
Robocasting alginate sacrificial substrate + PHBV Electrospinning	PHBV	Diameter: 0.5–2 mm	UTS: 0.6 MPa YS: 0.29 MPa Modulus: 15 MPa Elongation at break: 36.47% Suture retention strength: 41.67 MPa	Biodegradable PHBV vascular networks fabricated via the combination of robocasting and electrospinning techniques	Ortega et al.[50]
Co-extruding with 3D printed coaxial nozzles	F127-BUM	Diameter: 0.5, 2 mm Thickness: 0.15 mm	—	Hydrogel vascular tubes produced by 3D printed and fully customizable coaxial nozzles	Millik et al.[51]
Coaxial printing + LbL system	ε-polylysine/SA + Hep/YIGSR	Diameter: 0.6–1.2 mm Thickness: 0.2 mm	UTS: 0.2–0.33 MPa Modulus: 1–5 MPa Elongation at break: 5%–20%	Vascular constructs with a biologically inspired release system using the coaxial printing technique conjugated with electrostatic LbL technology	Zeng et al.[52]

(Continued)

Table 1. (Continued)

3D printing approach	Materials	Vascular construct size	Mechanical properties	Significance	References
Coaxial printing	Alginate + MWCNT	Diameter: 0.8–0.9 mm Thickness: 0.2 mm	UTS: 0.422 MPa Modulus: 15 MPa Elongation at break: 36.47% Suture retention strength: 41.67 MPa Burst pressure: 216–222 mmHg	Coaxially extruded cellular vascular conduits with reinforced mechanical properties by MWCNT	Zhang et al.[53]
Coaxial printing	GelMA/C + HCASMCs	Diameter: 5 mm Thickness: 0.4 mm Length: 5 cm	—	3D-printed free-standing, small diameter vasculature with smooth muscle and endothelium, hydrogels with smooth muscle and endothelial cells	Cui et al.[54]
Thermal inkjet printing	Alginate/gelatin + rat SMCs	Diameter: 2 mm Length: 2 mm	—	First developed cell-laden vascular constructs using a thermal inkjet printing process	Kesari et al.[55]
Thermal inkjet printing	Fibrinogen/thrombin + HMVECs	Diameter: 0.6 mm Thickness: 0.5 mm	UTS: 1.7 MPa Modulus: 2.9 MPa Burst pressure: 2955 mmHg	Inkjet printed human microvasculature with HMVECs	Cui and Boland[56]
Thermal inkjet printing	Alginate + PVA + HeLa Cells	—	—	3D vascular constructs manufactured by inkjetted SA beads with PVA as a viscosity enhancer	Nishiyama et al.[57]
Scaffold-free inkjet printing	Alginate + fibroblasts	Diameter: 3 mm Length: 0.5 cm	—	3D zigzag cellular tubes which have a controllable overhang structure by scaffold-free inkjet printing	Xu et al.[58]
Freeform inkjet printing	Alginate + fibroblasts	Diameter: 3 mm Thickness: 1 mm Length: 1 cm	—	3D complex tubular shape with a uniform diameter along horizontal and vertical directions using by freeform inkjet printing	Christensen et al.[59]
DLP based 3D printing	PPF	Diameter: 1 mm Thickness: 0.15 mm Length: 0.6 cm	UTS: 1.48–10 MPa Modulus: 8.79–20 MPa Elongation at break: 36.47% Burst pressure: 5000–16,000 mmHg	A customized vascular construct reconstructed via the 3D CAD model of defect derived from MRI or CT.	Melchiorri et al.[60]
DLP based 3D printing	PEGDA + HPM	Diameter: 6 mm Thickness: 1.5 mm	Modulus: 0.005–0.025 MPa	3D printed pericardium hydrogel based vascular constructs for wound healing	Bracaglia et al.[61]
DLP based 3D printing	ACMO + TMPTA + TMETA	Diameter: 4, 6 mm Thickness: 0.5 mm Length: 3 cm	UTS: 45 MPa Modulus: 110 MPa Elongation at break: 40% Suture retention force: 9 N Burst pressure: 250 mmHg	Arteriovenous graft for hemodialysis application using DLP based 3D printing	Bracaglia et al.[61]
DLP based 3D printing	Dopamine + HEMA	Diameter: 6 mm Thickness: 1 mm Length: 3.5 cm	Modulus: 3.456 MPa	Bi-layered and branched vascular constructs using DLP based 3D printing	Chiu et al.[62]
Wrapping cell sheet	Human skin fibroblasts	Diameter: 1.5, 4.5 mm Thickness: 0.2, 0.4 mm	Suture retention force: 1.6 N Compliance: 1.5%/100 mmHg Burst pressure: 3468–2688 mmHg	Human age- and risk-matched tissue-engineered blood vessels with complete tissue integration and vasa vasorum formation	L'Heureux et al.[63]
Casting cultured cells	Fibroblasts + fibrinogen	Diameter: 2, 4 mm Thickness: 0.3, 0.45 mm	Burst pressure: 596 mmHg	Casted tubular constructs remodeled by the fibroblasts with pulsed flow-stretch bioreactor	Syedain et al.[64]
Wrapping cell sheet	MSCs	Diameter: 2 mm Thickness: 0.5 mm Length: 1.5 cm	Suture retention strength: 25.8 MPa	Tissue-engineered vascular grafts from cultured marrow-derived MSCs	Zhao et al.[65]
iBTA	Fibroblasts of live dogs or goats	Diameter: 4, 5 mm Thickness: 0.8 mm Length: 25, 50 cm	UTS: 1.8 MPa Modulus: 7 MPa Elongation at break: 70% Suture retention force: 1.31 N Suture retention tension: 0.7 N/mm Burst pressure: 1500 mmHg	World's longest tissue-engineered vascular grafts using iBTA process	Nakayama et al.[66,67]
3D printing + the needle-array	HUVECs + HASMCs + HDFs	Diameter: 1.5 mm Length: 0.7 cm	Tension property: 939 mN	Combined both the needle-array and 3D printing systems for skewering the MCSs	Itoh et al.[68]
IDP	Alginate + polyacrylamide	Diameter: 3 mm Thickness: 0.8 mm Length: 2 cm	Modulus: 0.1–0.5 MPa Burst pressure: 100–250 mmHg	One-step printed vascular constructs with mechanical stability and perfusability	Zhou et al.[69]
EHD inkjet printing	GelMA + HDFs	Diameter: 0.03, 0.06 mm	—	Combination of sacrificial material strategy and an EHD inkjet printing for high resolution microvascular constructs	Zheng et al.[70]

layer stimulated fibroblast adhesion and proliferation, and a highly aligned inner layer with collagen allowed HUVECs to adhere and rapidly migrate, suggesting rapid endothelialization.

Recently, an advanced 3D printing system was introduced that uses a rotatable mandrel and an *XθZ*-axis instead of the conventional *XYZ*-axis.[43] The modified 3D printing system allowed the positive mandrel mold to be wrapped with a coil of alginate–gelatin for the fabrication of vessel-like tubular structures. Developed rotary forming method demonstrated higher accuracy and faster molding speed compared to the conventional deposition methods. Using a similar cylindrical mold, some researchers combined electrospinning and 3D printing systems for vascular construct applications.[44,45] Centola et al.[44] developed poly-L-lactide (PLLA)/PCL vascular constructs incorporated with heparin (Hep) using a combination of electrospinning and a fused deposition modeling-based 3D printing technique. The first process step was electrospinning of PLLA loaded with Hep for preventing thrombosis. Following this, the outer PCL coil structures were fabricated by 3D printing onto electrospun tubular PLLA/Hep. By coiling PCL, all of the mechanical property values remarkably increased and some values, such as burst pressure, suture retention force, and static compliance, were close to those of internal mammary arteries. PLLA/Hep/PCL vascular constructs induced differentiation of human mesenchymal stem cells (hMSCs) in ECs toward vascular endothelium. Meanwhile, another study introduced hybrid 3D-PCL constructs by combining electrospinning and 3D printing.[45] The fabricated constructs had a bilayered structure with an inner aligned nanofibrous layer and a stent-like outer layer, which were coated with polydopamine (PDA) and vascular endothelial growth factor (VEGF). The wettability of the vascular constructs was improved by PDA and the coating procedure did not substantially affect the mechanical properties of the vascular constructs. Lee et al. noted that the use of gentle aqueous conditions led to maintained structural integrity. The immobilized VEGF vascular constructs showed significantly improved angiogenic differentiation both in vitro and in vivo.

Sacrificial material strategy

Sacrificial support materials are widely used to shape permanent constructs. Using a sacrificial material that is easy to remove, a complex 3D structure can be formed with a second material, while the sacrificial material acts as a support matrix before being discarded. Sacrificial materials for vascular constructs have been produced by multiple methods including 3D printing techniques. Among the various sacrificial materials, water-soluble materials, such as sugar, sodium chloride (NaCl), and polyvinyl alcohol (PVA), are most commonly used because they are easily processed without contamination by residual organic solvents. Aligned sugar microfibers were melt-spun for use as sacrificial materials.[46] Sacrificial tubular sugar microfibers were filled with PLCL solution, and then the sugar microfiber template was dissolved in water. Random PLCL nanofibers were then covered onto aligned PLCL struts by electrospinning. After removal of the sugar microfibers, circumferentially aligned microchannels with high interconnectivity and porosity were obtained from within the vascular constructs. The tensile properties of the constructs, including UTS, elastic modulus, and strain at break, were superior to those of native arteries and the burst pressure of the constructs (1787 mmHg) was higher than that of saphenous veins (1700 mmHg). Oriented microchannels led to in vitro migration, oriented growth, elongation, and expression of the contractile protein of vascular smooth muscle cells (VSMCs). In vivo systems also simultaneously showed improved cell infiltration, oriented arrangement of VSMCs, aligned deposition of ECM fibrils, as well as polarization of macrophages, which indicated rapid endothelialization.

Water-soluble polymers such as PVA and polyethylene glycol (PEG) are attractive sacrificial support materials. In particular, PVA is a biodegradable thermoplastic that can be extruded at appropriate temperatures, thus it has already been manufactured as a filament for fused filament fabrication (FFF)-based 3D printing processes. Wang et al.[47] used a 3D printed PVA rod as a water-soluble sacrificial core for small-diameter vascular grafts. The 3D printed PVA core rod was coated with thermoplastic polyurethane (TPU) and NaCl solution by a sequential three-step dip coating method. Finally, the coated rod was immersed in distilled water to dissolve the PVA and NaCl granules. The fabricated vascular constructs were designed like native blood vessels and were composed of three layers: thin inner and outer layers with high porosity for cell adhesion and proliferation and a thick and compact middle layer that provided sufficient mechanical properties as a vascular construct. The triple-layered vascular constructs met all of the mechanical requirements, such as dynamic compliance, burst pressure, and suture retention strength, due to the compact middle layer that provided structure. Biological stability of the vascular constructs was confirmed by long-term in vivo tests using a sheep carotid arterial replacement model. Following implantation for 1 year, the vascular constructs showed better degradation and cell infiltration, but formed aneurysms caused by a mismatch between the degradation rate and tissue regeneration rate.

A similar experimental concept was conducted by Sohn et al.[48] They fabricated customized porous TPU vascular constructs using a sacrificial material strategy with 3D printing. PVA was used as the sacrificial material and was compared with a commercially available ePTFE vascular graft. Using NaCl as a porogen, the surface structure of the porous TPU vascular constructs had higher porosity than

that of the ePTFE graft. Endothelial cell activation, neovascularization, thrombus formation, calcification, inflammatory infiltrates, and fibrosis on the porous TPU vascular constructs were confirmed by animal experiments using a rat abdominal aorta model for 7 and 30 days. Compared to the ePTFE graft, a remarkable decrease in thrombogenesis was observed in the TPU vascular constructs after 30 days. The same group showed increased postoperative endothelialization in the early stages, demonstrating the possibility of clinical applications of the vascular constructs prepared by the sacrificial materials strategy. Even though improved properties of fabricated TPU grafts compared to commercial products were not noted, feasibility of this technique to clinical application with customized structures was represented. Recently, Park et al.[49] used a similar method with 3D printed PVA as the sacrificial support material, but the process was further developed and elaborated. To formulate a patient-customized whole vascular construct, 3D reconstructed images of native blood vessels were acquired by magnetic resonance imaging (MRI)—a representative medical imaging technology. Using fused deposition modeling (FDM)-based 3D printing, a blood vessel-like PVA core was fabricated, and PDMS was dip-coated on the core as the vascular construct material. In contrast with Zhou's study, aqueous hydrogen peroxide (H_2O_2) was used as a selective dissolving solution for the complete and rapid removal of the sacrificial PVA structure. H_2O_2 did not affect the chemical stability of PDMS, whereas it stimulated rapid dissolution of PVA by weakening the hydrogen bonds among the PVA chains. The hydroxyl and peroxyl radicals also increased the wettability of PDMS using distilled water. Moreover, the tensile properties of the PDMS construct were closely comparable to those of bare PDMS, suggesting that no mechanical degradation had occurred in the fabricated PDMS vascular constructs by the H_2O_2 solution.

Another study used the sacrificial material strategy with alginate, a linear, anionic polysaccharide hydrogel widely used for bioprinting. Ortega et al.[50] used alginate as the sacrificial material with ethylenediaminetetraacetic acid (EDTA) solution for degradation of the alginate. A poly(3-hydroxybutyrate-co-3-hydroxyvalerate) (PHBV) membrane was fabricated by electrospinning. An alginate/glycerol mixture was then patterned on the PHBV membrane by a robocasting technique for 3D printing, followed by layering another electrospun PHBV sheet. Poly(lactic-co-glycolic acid) (PLGA) was also electrospun onto the alginate pattern, and the alginate pattern between was degraded using EDTA solution. The scaffolds were well formed and the final vascular construct had sufficient mechanical properties. Both human dermal fibroblasts (HDFs) and human dermal microvascular ECs (HDMECs) were well-attached and showed uniform distribution within the vascular network surface. Produced simple vascular network will be beneficial to further develop the knowledge about neovascularization which was challenging by conventional in vitro tests.

Coaxial extrusion strategy

As reported above, general strategies include molding or sacrificial templating a synthetic or natural polymeric material around cylindrical shaped materials such as a mandrel or rod, in which the diameter of the mandrel or rod determines the vascular construct's luminal diameter. With rapid advancement of processes and technologies, numerous strategies have been devoted to producing vascular constructs with a perfusable tubular structure and appropriate performances for vascular applications. Recently, a coaxial extrusion strategy, a simple 3D printing technique, offered an easy approach to design tubular structures via a coaxial nozzle by tailoring the discharge of the 3D printing biomaterials. It was shown that coaxial extrusion could directly manufacture microchannel tubes with tunable diameters from micro to macro scale as well as large-scale lengths.

To design perfusable vascular constructs, 3D printed coaxial nozzles, prepared using a commercially available stereolithography (SLA) technique, were adapted to co-extrude hydrogel vascular constructs for enabling perfusion of engineered tissues and organs.[51] The Pluronic F127-bisurethane methacrylate (F127-BUM) hydrogel with collagen I and unmodified Pluronic F127 (F127) hydrogel were synthesized as the vascular conduit and sacrificial core materials, respectively. Vascular constructs were coextruded via the 3D printed coaxial nozzles combined with syringes. The syringe containing the sacrificial core hydrogel was affixed to the superior inlet and the syringe containing the outer permanent hydrogel was affixed to the lateral inlet. After coextrusion of the two materials, the outer hydrogel was photo-cured under a UV lamp and the sacrificial core hydrogel was removed through dissolution in aqueous medium to obtain hydrogel vascular constructs. Coextruded constructs had diameters of 0.5–2 mm and wall thicknesses of 150 μm. Their geometries could be customized by altering the coaxial nozzle size and shape as well as the coextrusion conditions such as pressure. Moreover, it was confirmed that HUVECs, which line the luminal surfaces of blood vessels, were well cultured on the luminal surfaces of the collagen I-treated F127-BUM hydrogel vascular constructs and yielded tubular endothelial monolayers, compared to the untreated hydrogels.

Similarly, other studies have reported hydrogel-based small-diameter vascular constructs prepared by coaxial extrusion technology. Zeng et al.[52] designed vascular constructs with a biologically inspired release system using the coaxial printing technique with electrostatic layer-by-layer (LbL) technology for antithrombogenicity and endothelialization. They used various combinations of

positively charged ε-polylysine (ε-PL) and negatively charged sodium alginate (SA) as the coaxial printing ink. The extruded hydrogel constructs were coated with dual bioactive molecules, Tyr-Ile-Gly-Ser-Arg (YIGSR)-peptide and Hep, via electrostatic LbL self-assembly. Uniform perfusable vascular constructs with a hollow structure were directly produced without any supporting core materials owing to the electrostatic interactions by the addition of ε-PL. The swelling and mechanical properties of the 3D printed ε-PL/SA vascular constructs were tuned by the composition of ε-PL and SA. Positively charged YIGSR and negatively charged Hep were successfully deposited LbL on the inner surface of the vascular constructs by the electrostatic interactions. The long-range electrostatic interactions allowed the Hep and YIGSR on the 3D printed ε-PL/SA vascular constructs to be sequentially released in a spatiotemporally coordinated manner. The different release behavior of Hep and YIGSR contributed to enhanced antithrombogenicity and endothelialization in vitro. Obtained vascular constructs with bioinspired release system by electrostatic interaction is regarded as highly promising for small-diameter vascular applications.

Zhang et al.[53] focused their research on the reinforcement of hydrogel-based vascular constructs, thus multiwall carbon nanotubes (MWCNTs) (0.5 and 1 w/v%) were used as reinforcement materials. Nitric acid treated MWCNTs (4 w/v%) were dispersed in SA hydrogel inks and the fabricated MWCNTs/SA hydrogels were extruded using coaxial nozzles. The addition of MWCNTs caused the dimensional values (i.e. diameter and wall thickness) of the hydrogel vascular constructs to decrease slightly, whereas no significant differences were observed in the swelling ratio, degradation rate, or perfusion capability between the control SA construct and the MWCNTs/SA construct. However, when 1 w/v% MWCNTs was dispersed in SA, the ultimate tensile strength and burst pressure were observed to increase by 10% compared to those of the control. In terms of biocompatibility, the addition of MWCNTs did not affect the short-term viability of human umbilical vein smooth muscle cells (HUVSMCs) in vitro compared to the control, but it hindered long-term HUVSMC survival as well as ECM formation in vitro. This restrained cellular behavior resulted from cytotoxicity of MWCNTs under prolonged physiological condition which should be resolved for further utilization.

In attempts to 3D-print free-standing, small-diameter vasculature with smooth muscle and endothelium, hydrogels containing smooth muscle and ECs were directly coextruded.[54] Catechol-functionalized gelatin methacrylate (GelMA/C) and F127 were chosen as the vascular construct and sacrificial core materials, respectively. A 20 wt% GelMA/C hydrogel combined with human coronary artery smooth muscle cells (HCASMCs) was extruded through an outer coaxial nozzle, whereas a fugitive slurry containing F127, sodium periodate ($NaIO_4$), and HUVECs flowed through an inner coaxial nozzle. The F127-based fugitive slurry was observed to act as a temporary supporter for the vascular constructs during coextrusion as well as an assistor in crosslinking the GelMA/C hydrogel. Furthermore, after removal of the fugitive slurry, it was confirmed that HUVECs could migrate and adhere to the inner surface of the GelMA/C hydrogel vascular construct. The crosslinked GelMA/C vascular constructs had controllable mechanical properties and high adhesion strength. The in vitro results indicated that the coextruded vascular constructs revealed numerous tissue-favorable, bioinspired characteristics such as manufacturing ability of vascularized tissue, proper vascular perfusability and permeability, and excellent vasculogenesis. Finally, the in vivo autonomous connection and vascular structure remodeling ensured the beneficial biocompatibility and implantation safety of the coextruded vascular constructs for further clinical application.

Inkjet printing strategy

Meanwhile, there are on-going attempts to incorporate cells into intermediate materials such as bioinks and obtain spatial control. Inkjet printing of cell-laden bioinks is an efficient method that allows a high density of cell loading with homogeneous cell distribution in the bioink, regardless of the number or type of cells. There are two types of inkjet printing techniques. The first is a continuous inkjet (CIJ) printing method in which a liquid binder is broken into a continuous stream of drops. The second is a drop-on-demand (DoD) printing method in which drops are ejected from a nozzle only when electrical signals are produced by a thermal or piezoelectric actuator. It is commonly used in bioprinting systems because of its good controllability and low contamination.

3D-printing cell-laden vascular constructs using a thermal inkjet printer was first developed at Clemson University in 2004.[55] A 0.25 M $CaCl_2$ solution ink was printed as a vascular construct pattern onto a mixture of SA and gelatin in a chamber, then rat SMCs were pipetted onto the crosslinked SA/gelatin tubular constructs. After culturing the SA/gelatin tubular constructs with encapsulated SMCs up to 18 days, the SMCs in the vascular constructs were well distributed and viable. Moreover, functional responses were observed in vitro, suggesting that the use of inkjet-based 3D printing to construct vascular structures has much potential. The research team attempted to use fibrin as an inkjet printing material, which could play an important role in blood clotting, wound healing, and angiogenesis.[56] The optimized fibrinogen and thrombin solution with human microvascular endothelial cells (HMVECs) was deposited on the fibrin gel by a thermal inkjet printer. The fabricated fibrin fibers were well aligned and straight, and showed open hollow channels

that could promote cell attachment and proliferation. They exhibited appropriate UTS (1.7 ± 0.5 MPa) and Young's modulus (2.9 ± 0.8 MPa) values, and a burst pressure (2955 mmHg) similar to the average burst pressure of tissue-engineered blood vessels (TEBVs) (3340 mmHg). 3D printed HMVECs were well seeded and proliferated on the fibrin gel, and self-aligned in the fibrin channels that formed the human microvasculature. The integrity of HMVECs on the 3D printed vascular structure was maintained for 3 weeks of culturing.

On the other hand, Nishiyama et al.[57] used PVA as a viscosity enhancer in SA hydrogel. Because the inkjetted SA beads suspended in a low viscosity substrate moved arbitrarily, a SA gel structure could not be fabricated with precise positioning. Thus, a mixture of SA and PVA loaded with HeLa cells was ejected using the inkjet-based 3D printer. 3D vascular constructs were successfully produced by continuously drawing around the same position as the hydrogel loops were stacked to form 3D vascular constructs. In particular, when more than 15% of PVA was used, the mixture exhibited good supporting properties for the 3D constructs. However, it was confirmed that only 70% of the cells were alive after 3D printing.

Xu et al.[58] designed a scaffold-free inkjet printing system for printing vessel-like 3D cellular constructs. They proposed complex 3D constructs, such as a zigzag tubular construct with a controllable overhang structure. NIH 3T3 mouse fibroblasts (3T3 cells) and SA were used as the bioink to bioprint cell-laden vascular constructs using a piezoelectric inkjet printer. Bioinks consisting of 3T3 cells suspended in SA were printed in a $CaCl_2$ solution bath to form sequentially crosslinked tubular layers. By decreasing the dispenser head speed, a stable continuous hydrogel strand could be formed and 210 layers of bioinks were successfully deposited for the zigzag tubular structure possessing a rugged overhang structure with an angle and height of 63° and 5 mm, respectively. The cell viability of the 3T3 cells in the printed constructs was slightly lower than that of the control due to the high shear stress applied to the cells during the inkjet printing. However, even after 72 h of incubation, the cell viability remained above 93%, demonstrating the promising approach of the proposed inkjet printing system. Based on the previous procedure, Christensen et al.[59] confirmed the feasibility of scaffold-free inkjet printing of vascular constructs with both horizontal and vertical bifurcations. In this study, $CaCl_2$ solution was used for gelling the SA hydrogels and supporting the 3D printed structures. Consequently, a complex 3D tubular shape with a uniform diameter along the horizontal and vertical directions was formed, with the solution providing a supporting buoyant force. The 3T3 cell viability of the printed vascular constructs was 90.8% immediately after printing and 92.4% after 24 h of incubation. Cellularly heterogeneous vasculature with considerably complicated structure would also be possible by utilizing the demonstrated drop-wise fabrication method with more advancements.

Lithography-based printing strategy

Photolithography-based 3D printing techniques, such as digital light processing (DLP) and SLA, are some of the most promising alternative approaches for transforming photocurable synthetic biopolymers into complex 3D constructs. It is noteworthy that these techniques offer liquid-based supporting materials during the 3D printing process and permit high spatial resolution exceeding that of other 3D printing approaches (such as extrusion-based printing), thereby providing the potential to well-engineer the complex architecture and micro-environment of artificial organs. Particularly, there have been multiple attempts to fabricate complex vascular constructs using DLP technology, in which UV light was projected onto a mirror array. Melchiorri et al.[60] developed 3D printed biodegradable polymeric vascular constructs for congenital heart disease applications. Polypropylene fumarate (PPF), a biocompatible and biodegradable polyester, was chosen as a photocurable polymer and was mixed with other additives such as a photoinitiator. A customized vascular construct model was reconstructed via a 3D computer-aided design (CAD) model of defect derived from MRI or computer tomography (CT). Finally, a vascular construct with a length of 6.0 mm, inner diameter of 1 mm, and wall thickness of 0.15 mm was 3D printed under a UV light DLP system. As the UV light exposure (based on flashes of light) increased from 100 to 2000 flashes, the UTS and elastic modulus of the 3D printed PPF vascular constructs also increased. Furthermore, the mechanical properties of the specimen after 500 flashes of the UV lamp were comparable to those of the saphenous vein and femoral artery, usually used in grafting procedures and appropriate for use as venous grafts. In vitro and in vivo biodegradation tests showed that the 3D printed PPF vascular constructs maintained mechanical and physicochemical stability even after 6 months. Additionally, no thrombosis, graft aneurysm, or stenosis was observed in vivo throughout the implantation period.

Meanwhile, DLP printing technology was applied to fabricate pericardium hydrogel-based vascular constructs for wound healing.[61] The pericardium, also called pericardial sac, is a double-walled dense tissue that contains the heart and vascular vessels. It consists of various fiber proteins, which offer appropriate tensile properties, as well as glycans, such as collagen, elastin, fibronectin, and fibrillin, which promote cell adhesion for cell matrix interactions. Therefore, by chemically combining polyethylene glycol acrylate (PEGDA) and homogenized decellularized bovine pericardium matrix (HPM), bioactive hydrogel vascular constructs were fabricated with the capability to moderate inflammatory responses and support HUVEC growth.

Cross-linkable hydrogels were synthesized with HPM, PEGDA, and other additives, then curved and branched vascular constructs (6 mm inner diameter and 1.5 mm wall thickness) were obtained by the DLP based 3D printing process. The addition of stiff and bioactive HPM in the PEGDA hydrogels increased the compressive modulus of the hybrid hydrogels, while decreasing inflammatory cytokines, such as TNFα and IL1β, during coculture experiments, indicating that the HPM reduced the inflammatory response and provided a healing environment for HUVECs.

Acrylate polymers have been widely used as photolithography-based 3D printing materials owing to their high-speed crosslinking reactions, in which acrylic-based liquid resin solidifies via the establishment of acrylic bonds after exposure to UV light. Thus, there are various studies demonstrating the potential of 3D printed acrylate copolymers and acrylic polymers using the DLP system for vascular applications. Cheng et al.[71] examined two different acrylate copolymers for arteriovenous graft (AVG) applications. Modified 4-acryloylmorpholine (ACMO) with trimethylolpropane triacrylate (TMPTA) and trimethylolpropane ethoxylate triacrylate (TMETA) was used as a 3D printing ink and PEGDA was used as a control material. ACMO was incorporated in the ink to adopt its intrinsic characteristics which include inhibiting protein adsorption and anti-fouling property for fabricating functionalized vascular grafts. The DLP process easily formed small-diameter ACMO vascular constructs (ACMO-AVG) with smooth surfaces and diameters of 4 or 6 mm. 3D printed ACMO vascular constructs displayed better mechanical stability, in terms of tensile and suture retention strength and fracture energy, than PEGDA constructs. The structural stability and biocompatibility of ACMO-AVG were also confirmed by in vitro fluidic tests and fibroblast toxicity tests. Moreover, ACMO-AVG exhibited anti-fouling characteristics that prohibited plasma protein adsorption and platelet adhesion, as well as prevented endothelialization on the luminal surfaces of ACMO-AVG.

Chiu et al.[62] used the DLP system to 3D-print a photocurable amine-based resin (AR) for vascular engineering applications. A natural dopamine (DA) and 2-hydroxylethyl methacrylate (HEMA) were used as light absorbers to enhance the 3D printing resolution. Bilayered and branched vascular constructs with diameters of 6 mm and wall thicknesses of 1 mm were 3D printed through the DLP 3D printer. By tailoring the ratio of AR, HEMA, and DA, as well as the curing durations, the Young's modulus values of the fabricated vascular constructs were in the range of 0.701–0.983 MPa, which were close to those of native blood vessels. The various experimental conditions affected the printing accuracy as well as the cell viability of the 3D printed vascular constructs. Identified relation between printing parameters and obtained results is useful for setting optimal printing conditions. Moreover, adopting dopamine for artificial blood vessels is also notable.

Others

Some researchers have used cultured cell tissues directly for engineering vascular alternatives of native blood vessels. Cultured human skin fibroblasts (HSFs) on gelatin were wrapped around a stainless steel mandrel to construct human age- and risk-matched TEBVs.[63] Although the TEBV construct was based on cultured cells, it showed mechanical properties comparable to those of human blood vessels and the mechanical stability of TEBVs was maintained for up to 8 months in vivo. Histological results demonstrated complete tissue integration and vasa vasorum formation. As autologous TEBVs are the ideal grafts for substituting vessels, developing vascular grafts are worth the long preparation time (~28 weeks). Tissue-engineered arteries were also fabricated by the entrapment of HDFs in fibrin gel.[64] The suspended fibroblasts/fibrinogen was injected into a tubular mold and then cultured for 2 weeks to achieve stiffening and strengthening of the vascular grafts. After 9 weeks of culturing in a handmade bioreactor with pulsed flow, the casted tubular constructs were remodeled by the fibroblasts into circumferentially stretched tubes of collagen and other ECMs with predictable burst pressures. The cultured vascular constructs with 2 mm diameters possessed suture retention strength and compliance comparable to those of native rat aorta. Meanwhile, Zhao et al.[65] fabricated tissue-engineered vascular grafts (TEVGs) by rolling a sheet of marrow MSC around a mandrel. The cultured TEVGs were implanted into a rabbit carotid artery. After 4 weeks, the TEVGs were well integrated with the artery vessel and showed excellent patency.

Nakayama et al.[66] investigated long in vivo tissue-engineered vascular constructs called "Biotubes." They designed spiral-shaped molds that consist of an outer pipe-shaped spiral shell and an inner spiral mandrel prepared by casting nylon. The casted spiral molds were subcutaneously inserted into dogs or goats to form in-body tissue architecture (iBTA) during an in-body incubation period. Following extraction of the spiral molds, the space between the outer pipe and inner spiral mandrel was completely filled with collagen fibers with some fibroblast cells, thus fabricating autologous implantable vascular constructs. At the time of printing, Biotubes of 50 cm in length were the world's longest vascular constructs, with 60% of the strength and burst pressure values of native carotid arteries and 1/8th of the tensile property values (including UTS and elastic modulus) of native carotid arteries. Although Biotubes showed relatively poor mechanical properties compared to carotid arteries, autologously implanted Biotubes showed smooth blood flow and no apparent thrombus formation without additional

luminal modification or mechanical support, demonstrating the potential of the iBTA-based molding technique to develop vascular constructs that are hemocompatible. The research team also confirmed the use of Biotubes in clinical practice.[67] Biotubes with diameters of 6 mm and total lengths of 7 cm were similarly produced by implantation for 2 months in the abdominal subcutaneous tissue of patients who were undergoing hemodialysis. Although the implanted Biotubes led to stenosis for patients 4 months after the first surgery, this study has clinical significance because the first human case study was performed using autologous vascular constructs prepared by a molding technique.

Recently, various researchers have proposed novel 3D printing techniques that differ from conventional 3D printing for constructing vascular structures. Itoh et al.[68] added a 9×9 needle-array in the "Bio-3D printer"-based system to create freeform vascular constructs. Multicellular spheroids (MCSs) composed of HUVECs, human aortic smooth muscle cells (HASMCs), and HDFs were 3D printed into the needle-array with a 3D tubular structure, then the needle-array was removed after culturing for 4 days. The skewered MCSs formed a tubular shape, and holes in the pierced MCSs made by the needle-array were completely closed after pre-incubation. Directly printed MCSs were well distributed in the tubular tissues, and the luminal surface of the vascular constructs was covered with ECs after implantation into nude rats. Although the mechanical property (939 mN) of the fabricated vascular construct was about half of the value of native vessels, it should be noted that the spheroids were 3D printed by a modified 3D printing system without supporting materials.

Zhou et al.[69] developed a one-step printing process called the interfacial diffusion printing (IDP) process for manufacturing artificial vascular constructs. Once mixed, the SA and polyacrylamide hydrogel is printed into the curing reservoir filled with N,N,N′,N′-tetramethylethylenediamine (TEMED) and $CaCl_2$ solution as the curing agents. The rapid chelating reaction between SA and $CaCl_2$ accounts for the formation of a thin layer, which becomes a crosslinked interface that separates the inner precursors from the outer curing agents. Then, the $CaCl_2$ immediately diffuses through the interface, which leads to the formation of a thick hydrogel wall that mostly fixes the shape of the hydrogel strand. Simultaneously, TEMED can also diffuse into the inner ink to generate free radicals with acrylamide polymerization, which initiates the gelation of acrylamide and induces the formation of the second network. Due to step-wise fabrication process, variables of tubes including diameter and thickness were easily controllable. The geometrical specifications of the vascular construct are tailored by the nozzle size and reaction time. The mechanical properties of the constructs were similar to those of native blood vessels in terms of rheological, tensile, and compression tests, suggesting that the addition of bacterial cellulose provided extra hydrogen bonds for double crosslinking hydrogel constructs. Vascular constructs have shown satisfactory blood compatibility and cell biocompatibility in vitro. In the animal model, it was confirmed that the implanted vascular constructs were mechanically stable and perfusable in rabbit carotid artery replacement without any sign of inflammation up to 1 month.

More recently, Zheng et al.[70] combined the sacrificial material strategy with electrohydrodynamic (EHD) inkjet printing, a DoD inkjet printing technique with considerably smaller droplets, to fabricate high resolution microvascular constructs with hierarchical and branching channels. In their study, GelMA and F127 served as the permanent matrix and sacrificial material, respectively. The F127 ink was loaded into a glass capillary nozzle with tip diameter of 2–2.5 μm, and then deposited onto a PDA treated PDMS substrate. GelMA hydrogel (15 wt%) containing suspended HDFs was crosslinked at 37°C under UV light onto the F127 printed PDA-treated PDMS. After inserting the nozzle at positions of inlet and outlet, the fabricated constructs were cooled to 4°C to remove the F127 hydrogel. Finally, HUVECs were seeded on the fibronectin-coated internal surfaces of the microchannels. Perfusable microvascular constructs were successfully engineered by EHD inkjet printing with high resolution (the resolution scale was 30 μm, which approaches the physical scale of native capillary blood vessels). HDFs and HUVECs were co-cultured within the tailored microvascular constructs for up to 21 days, and the cultured cells with the microvascular constructs exhibited significantly higher viability ($>$90%) than the control group. The EHD inkjet printing technique provides a novel strategy for developing complex and delicate vascular constructs with the potential to adapt to an artificial organ model.

Freeform 3D printing technologies for artificial tissues with vascularized structures

Although conventional techniques to fabricate artificial vasculature have reported promising results for substituting damaged blood vessels, limitations remain. Since the ultimate purpose of fabricating vascularized structures resides in creating structures that are biomimetic, production methods should have the ability to generate highly complicated structures. However, it is challenging to achieve this through printing since self-supporting structures eventually collapse without supporting materials to withstand the weight of the vasculature. To overcome the abovementioned limitation, freeform 3D printing technologies for generating vascularized structures have been extensively studied using various strategies and materials. In this section, freeform 3D printing technologies are

classified into (i) material extrusion-based freeform 3D printing technologies, (ii) cell-laden ink extrusion-based 3D freeform 3D printing technologies, (iii) cell construct-based 3D freeform 3D printing technologies, (iv) photodegradation-based 3D freeform 3D printing technologies, and (v) projection SLA-based 3D freeform 3D printing technologies following the methodological characteristics as illustrated in Figure 3. Studies regarding each technology have adopted a diverse range of materials for the printing ink and the supporting bath or matrix to generate freeform-channeled structures for vascularization as summarized in Table 2.

Material extrusion-based freeform 3D printing technologies

Material extrusion-based 3D freeform 3D printing systems are comprised of a supporting bath that prohibits the collapse of the printed material with complex shapes, and a degradable ink that generates channels after perfusion. The cell-containing medium is infiltrated into the channels for cell growth in the inner space of the printed material. Therefore, the printability of the perfusable ink in the supporting bath and the biocompatibility of the residual material after perfusion are the key issues for this technology.

Wu et al.[34] reported omnidirectional printing (ODP) of 3D microchannels for vascular applications using F127 and chemically modified F127 (Figure 4). Although pure F127 exhibited suitable characteristics for the reservoir to withstand the weight of the printed material during printing, it was too weak to maintain the structure after removal of the ink. Thus, they chemically modified F127 by exchanging terminal groups with diacrylate groups to produce Pluronic F127 diacrylate (F127-DA). F127-DA was adopted as the reservoir material at a concentration that achieved viscosity and G′ comparable to those of pure F127. The terminal diacrylate groups of F127-DA could be photo-crosslinked under UV light (365 nm), which was unobtainable with pure F127. The channel diameter was controlled by adjusting the applied pressure to the nozzle. A linear increase in the channel size was found to follow the increase in pressure at each nozzle diameter. In particular, they noted that microchannels (18–70 μm) were achieved by varying the pressure to the nozzle with a 30 μm diameter. Assessment of the diffusion through the hydrogel matrix was conducted using rhodamine-based fluorescent dye injected into 125 μm microchannels. The results confirmed that the calculated diffusion rate was consistent with the reported values. Due to the usefulness of F127, research regarding F127 as a channel generator within cell-laden microgel matrices was conducted.[72] Molley et al. investigated artificial vasculature using F127 as a sacrificial ink inside the cell-laden GelMA bath. Specifically positioning cells within the matrix was also possible through the developed system. GelMA microparticles were fabricated through a water-in-oil emulsion technique, and the average diameter of the microparticles was 100 μm. Adipose derived stem cells were seeded on both the bulk GelMA hydrogel and GelMA microparticles to assess the change in cellular volume. Interestingly, the cell volume in the GelMA microparticles was greater than that in the bulk hydrogel, which suggested viability and bioactivity of the network. After preparation of GelMA microparticles, solidified F127 was inserted into the GelMA bath followed by photocrosslinking of the GelMA to harden the supporting bath. Subsequently, microgel containing F127 was refrigerated to liquefy and remove the F127, with the remaining channels having diameters of 300–600 μm. HUVECs were injected to vascularize through the channels, which led to the luminal surfaces of the channels being covered with HUVECs. However, some areas without HUVECs were observed due to the gaps that remained between the GelMA microparticles. Furthermore, they demonstrated a novel tumor invasion model using the established platform with the vascular channels and B16 mouse melanoma tumor cells.

Gelatin or modified gelatin-based supporting baths are prevalent in freeform 3D printing studies. A research article by Compaan et al.[73] is a representative study that made use of a cross-linkable gelatin-gellan microgel bath. In this research, gellan and gelatin microgels were independently fabricated to form a solid-like matrix bath under a gelatin-based precursor used to control the rheology. Although the supporting matrix exhibited solid-like behavior, it liquefied by shear stress, which enabled 3D printing of the alginate sacrificial ink. After deposition, microgels gathered around the sacrificial ink and this phenomenon aided the stability of the ink inside the supporting bath. Then, the gelatin-based continuous phase in the matrix was chemically crosslinked by transglutaminase (TG) to harden the established freeform structure. Finally, the alginate sacrificial ink was eliminated, leaving channels with 0.75–1 mm diameters. Pure gelatin without chemical modifications was used to exclude potential harmful effects during UV irradiation. Calcium cations were necessary within the matrix bath to prevent deterioration of the deposited ink by reduction of ink diffusion since the sacrificial ink was alginate. However, the authors commented that the incorporation of cells in this system was quite limited because TG, which eventually crosslinks the matrix, could be deactivated by the culturing medium. The low throughput and low penetration depth limit the ability to apply this method to larger constructs, although the method can rapidly generate channeled freeform networks. Additionally, gelatin granules from porcine skin after grinding were adopted for the matrix, under which xanthan gum (XG)-based filaments were deposited using the freeform reversible embedding of suspended hydrogels (FRESH) method.[74] The sacrificial ink was based on water-soluble XG and a

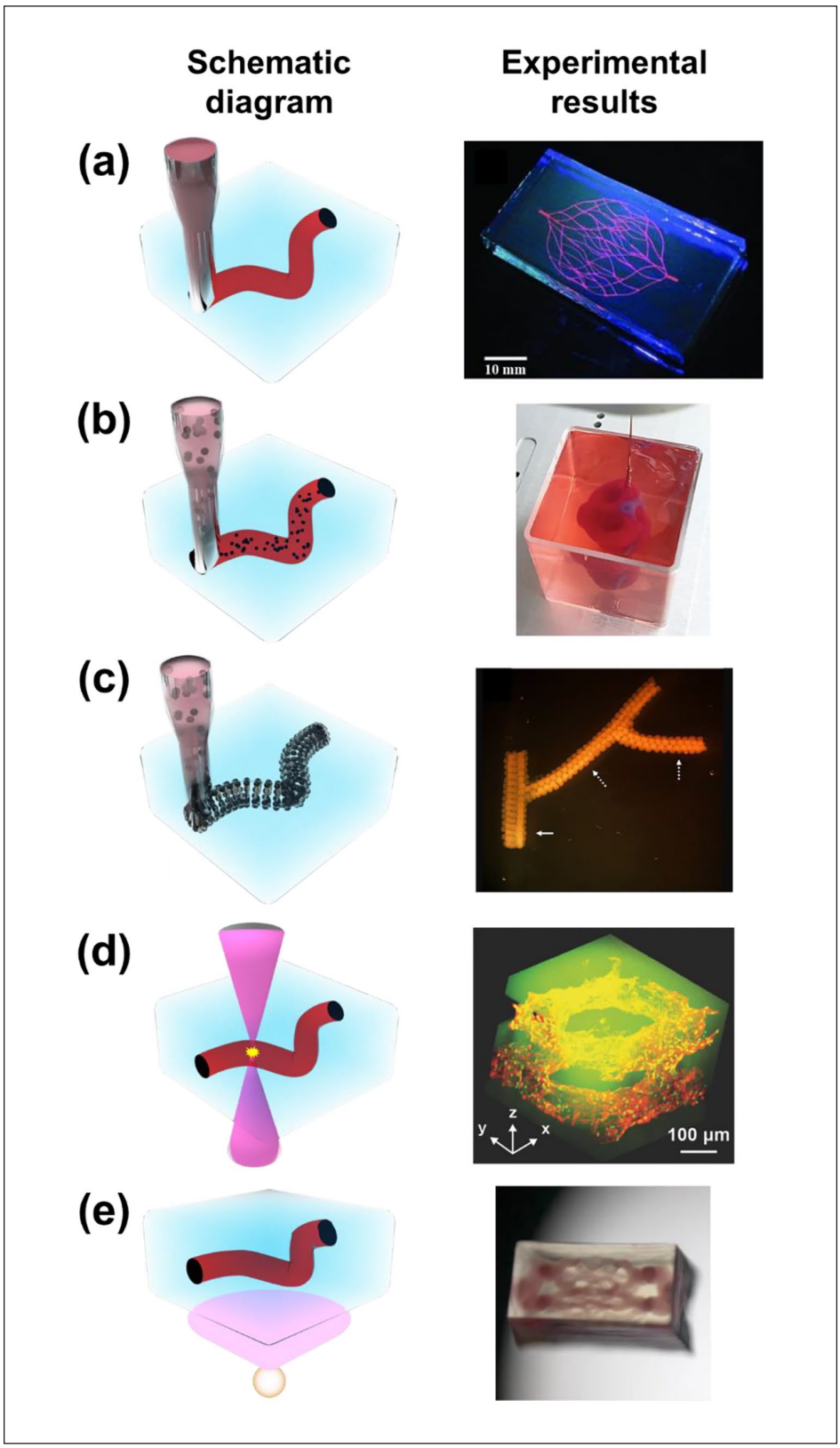

Figure 3. Schematic diagram and typical experimental results of (a) material extrusion-based freeform 3D printing (adapted with permission from Wu et al.[34]), (b) cell-laden ink extrusion-based freeform 3D printing (adapted with permission from Noor et al.[77]), (c) cell construct-based freeform 3D printing (adapted with permission from Norotte et al.[80]), (d) photodegradation-based freeform 3D printing (adapted with permission from Arakawa et al.[85]), and (e) projection stereolithography-based freeform 3D printing (adapted with permission from Thomas et al.[88]).

Table 2. Summary of freeform 3D printing strategies for vascular applications.

3D printing approach	Printing materials	Supporting materials	Vascular construct size	Significance	References
ODP	F127	F127-DA	Diameter: 18–170 μm (30 μm glass capillary) ~600 μm (200 μm SUS nozzle)	3D biomimetic micro-vascular networks embedded within a hydrogel matrix via omnidirectional printing	Wu et al.[34]
Extrusion 3D printing	F127	GelMA microparticle	Diameter : 300–600 μm (410 μm nozzle)	Complex processes like tumor intravasation and extravasation, and accompanying roles of stroma-cancer cell interaction, can be readily modeled.	Molley et al.[72]
Embedding printing	Alginate solution	Gellan and gelatin based microgel	Diameter : 750–1000 μm (840 μm nozzle)	Design and test a cross-linkable microgel composite matrix bath for embedded bioprinting of perfusable tissue constructs as well as sculpting of solid objects	Compaan et al.[73]
FRESH	Xanthan-gum	Gelatin granules, alginate granules	Diameter : 600 μm (210 μm nozzle)	Fabrication of perfusable freeform microfluidics, created from hydrogels based on biopolymers	Štumberger and Vihar[74]
3D injection	Photocrosslinkable PVA, Sylgard 184	Carbopol ETD 2020 granules, Dow Corning 9041 silicone elastomer granules	Diameter : 100 μm or larger wall thickness: 100 μm or larger (50 μm glass microcapillary)	Remarkable properties of the soft granular gel medium provide stability and versatility within an easy framework	Bhattacharjee et al.[75]
Syringe-based coaxial extrusion	Photocrosslinkable bioelastomer prepolymers based on ITA	Carbomer 940 hydrogel	Diameter : 500 ± 67 μm Wall thickness : 100–200 μm (1260 μm outer diameter/600 μm inner diameter)	Synthesized new bioelastomers based on ITA and printed perfusable tubular structure exhibited structural integrity	Savoji et al.[76]
Extrusion-based printing	dECM + iPSC-derived CMs, gelatin + ECs	Alginate solution + xanthan gum	Diameter : ~200 μm (140 μm needle)	The use of fully personalized, nonsupplemented materials as bioinks for 3D printing. Demonstrating the potential of the approach for organ replacement after failure, or for drug screening in an appropriate anatomical structure	Noor et al.[77]
Extrusion-based printing	GelMA, MeTro + CMs/CFs/ HUVECs	Carbopol gel	Diameter : 3 mm Wall thickness : 350 μm (340 μm nozzle)	Combination of GelMA and MeTro resulted in high-resolution printing with great cell viability.	Lee et al.[78]
Extrusion-based printing	Alginate + NIH-3T3 cells	F127 + Laponite-RDS	Diameter : 5 mm Wall thickness : 950 μm (260 μm nozzle)	Supporting gel based on PF-RDS allowed precise printing, helped recovery of the structures, and provided cell friendly environment.	Afghah et al.[79]
Extrusion-based printing	Alginate + L929 cells	XG-GMA + L929 cells	Diameter : 340 μm (260 μm needle)	New supporting material for up-scaling embedded 3D bio-printing technology that was implemented with xanthan gum, a biocompatible, wide accessible, and low cost natural polysaccharide	Patrício et al.[27]

(Continued)

Table 2. (Continued)

3D printing approach	Printing materials	Supporting materials	Vascular construct size	Significance	References
Scaffold-free rapid prototyping	Multicellular spheroids	Agarose rods	Diameter : 0.9–2.5 mm (300 or 500 μm micropipettes)	Patterning of distinct cell types to construct structures that are both compositionally and architecturally intricate	Norotte et al.[80]
Extrusion-based printing	Multicellular organoids (iPSCs)	Gelatin-fibrinogen ECM	Diameter : 132 μm and 182 μm (50 and 100 μm metal nozzle)	Fragile cells such as primary stem cells can be organized into a complex geometry directly within the most potent 3D culture matrices	Skylar-Scott et al.[81]
SWIFT	Gelatin	OBBs containing iPSCs-derived	Diameter : 400 μm (250 μm metal nozzle)	Demonstrated SWIFT method that uses iPSC-derived OBB tissue matrices that exhibit the requisite cell density, microarchitecture, and function approaching that of native tissues	Skylar-Scott et al.[82]
Multiphoton micromachining	—	Silk hydrogel + hMSCs	Diameter : >5 μm	Rapid formation of high-resolution structures over multiple length scales in three dimensions and could be carried out in cell-laden hydrogels	Applegate et al.[83]
Laser ablation	—	PEG hydrogel, Collagen I hydrogel + mouse myoblast cell line (C_2C_{12}), HUVECs, MSCs	Diameter : >2 μm	No complex steps are involved in the fabrication of microfluidic networks with guaranteed sterility of the cell cultures.	Brandenberg and Lutolf[84]
Multiphoton photodegradation	—	PEG-tetraBCN with the diazide N_3-oNB-RGPQGIWGQGRGDSGK(N_3)-NH_2 peptide + human bone marrow-derived hS5 stromal cells, HUVECs	Diameter : >10 μm	Multiphoton-assisted photodegradation enables fabrication and subsequent modification of complex endothelialized 3D micro-vascular networks with customizable intraluminal architectures in the presence of encapsulated cells.	Arakawa et al.[85]
μCOB	GM-HA, GelMA + HUVECs, 10T1/2 cells, HepG2 cells	GelMA	Diameter : 50–250 μm	Superior ability of computer-aided photopolymerization-based 3D bioprinting system Anastomosis between the grafted prevascularized tissues and the host vasculature was observed indicating the formation of functional vasculature in engineered tissues	Zhu et al.[86]
SLATE	Collagen solution + HUVECs, primary hepatocytes	PEGDA, GelMA	Diameter : >50 μm	Soft granular gel medium provide stability and versatility within an easy framework	Grigoryan et al.[87]
Projection-based multi-material stereolithographic bioprinting	HAMA	GelMA	Diameter : 360−720 μm Height : 360 μm	Screening multiple photoink formulations based on hyaluronic acid for sacrificial material system for stereolithographic bioprinting and subsequent digestion	Thomas et al.[88]

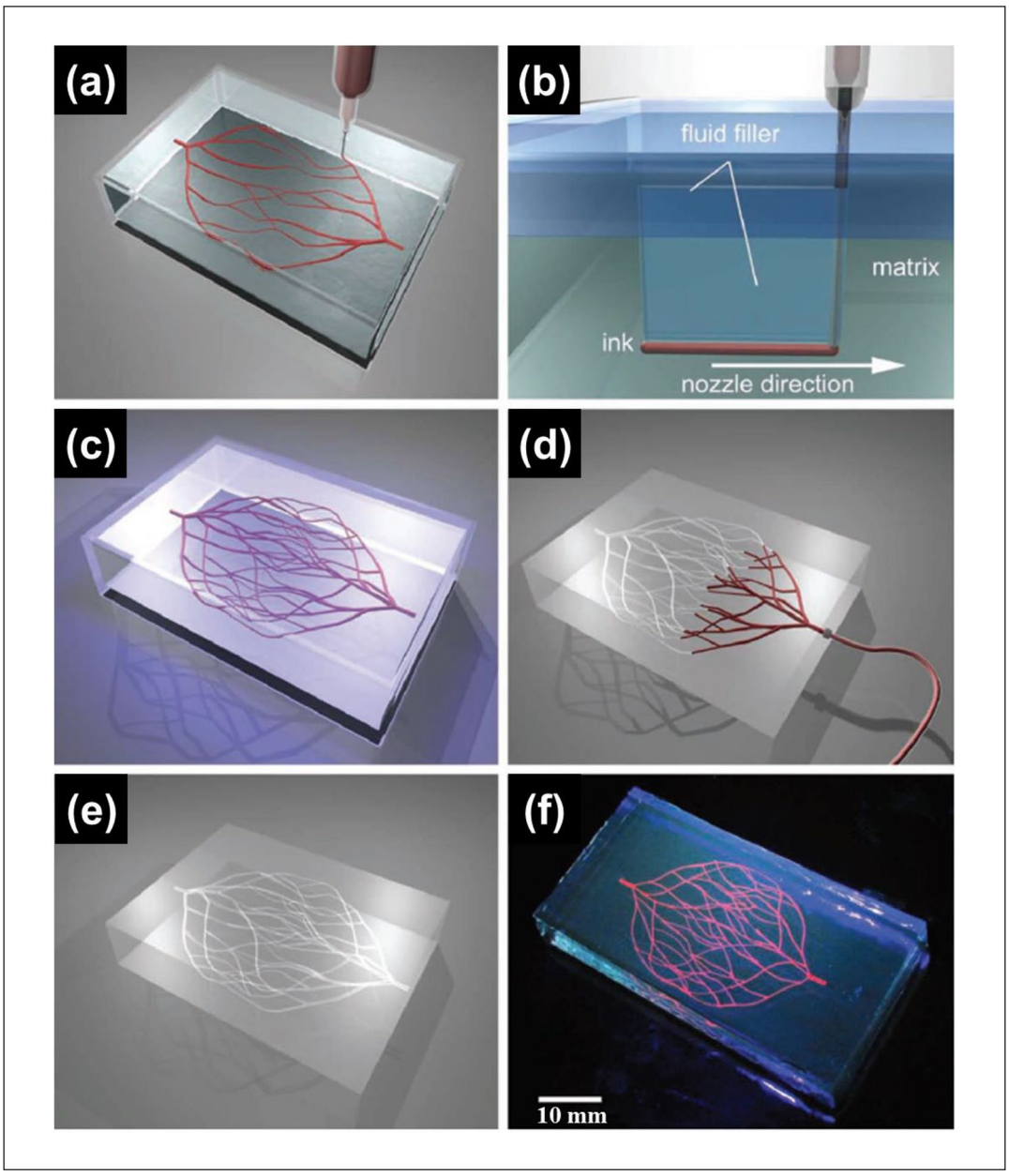

Figure 4. Schematics of ODP of 3D microvascular networks within a hydrogel fluid. (a) Hierarchical and branching networks of sacrificial ink patterned in a gel fluid. (b) Voids induced by nozzle movement are filled with liquid that migrates from the fluid capping layer. (c) Photopolymerization of supporting fluid to get crosslinked hydrogel supporting matrix. (d and e) Microvascular channels were evacuated by applying modest vacuum to liquefied ink. (f) Fluorescent image of a 3D microvascular network fabricated via omnidirectional printing of a sacrificial ink (dyed red) within a photopolymerized F127-diacrylate matrix.
Source: Adapted with permission from Wu et al.[34]

channel of about 0.6 mm was created using G27 nozzles (0.21 mm inner diameter). Another interesting aspect of this research was the demonstration of an alginate granule-based matrix with a substituted gelatin matrix.

Some commercial products have also proved to be useful as a supporting bath in freeform 3D printing. Commercially available Carbopol ETD 2020 polymer solution and Carbomer 940 hydrogel were utilized as supporting materials to create a freeform 3D vascular structure. The study utilized Carbopol microgels and found that they possessed excellent characteristics, including exceedingly low yield stress and viscosity, and they solidified at an extraordinarily low concentration.[75,76] Using the unique supporting microgel bath, freeform 3D printability was demonstrated for PVA, SA, hyaluronic acid, polyacrylamide, and PEG. Strikingly, after removal of the granular gel, the printed jellyfish model could float in water with high stability and flexibility. The highly precise

structure was generated using 50 μm injection tips on glass microcapillaries. Moreover, the possibility of direct cell printing was shown by assessing the 3D distribution of living human aortic ECs (HAECs) along the printing path, resulting from the excellent biocompatibility of the granular gel. Although limitations remain in this method, it should be noted that simple media preparation could overcome the barriers to producing highly complex structures without unnecessary supports. Savoji et al.[76] reported fabrication of vascular tubes using synthesized photocrosslinkable bioelastomers in the Carbomer hydrogel bath. Similar to other freeform 3D printing methods, washing of the hydrogel bath was followed by photocrosslinking of bioelastomers by UV irradiation. Through chemical reaction, they developed new photocrosslinkable bioelastomer prepolymers comprised of dimethyl itaconate (DMI), triethyl citrate (TEC), itaconate (ITA), and 1,8-octanediol. Additionally, they achieved a nanoporous structure by embedding poly(ethylene glycol)dimethyl ether (PEGDM) in the prepolymer solution. Fabrication of the tubular structure was carried out using a modified FFF printer with 3D coaxial printing feasibility (the Carbomer gel was placed inside and the bioelastomer was placed outside) in the Carbomer hydrogel bath. Once the entire printing process was finished, photocrosslinking was followed by exposure to UV light (365 nm, Irgacure 2959) and subsequently the structure was rinsed with PBS to liquefy the Carbomer hydrogel. All of the created bioelastomer prepolymers exhibited comparable cell viability to that of tissue culture plates, which represents potential applications in soft-tissue engineering. Superior permeability was observed in the bioelastomers compared to microvessels. UV light sensitivity was different in each of the developed prepolymers, which could be applied to other freeform 3D printing systems to achieve rheological behavior comparable to that of the chosen bath material. The porous structure obtained using the PEGDM embedded solution had a hierarchical structure, which would permit easier transport of nutrients. Moreover, clear endothelialization was observed in the bioelastomer tubes with HUVECs and the feasibility of supporting cardiac tissue in the tubes was demonstrated using human pluripotent stem cell (hPSC)-derived cardiomyocytes (CMs).

Cell-laden ink extrusion-based freeform 3D printing technologies

Inspired by material extrusion-based freeform 3D printing, studies of supplementing cells in biocompatible materials for freeform 3D printing have been widely conducted. For cell-laden ink extrusion-based freeform 3D printing technologies, materials for the ink and supporting bath should be biocompatible to ensure cell viability. The printing procedure must be carefully controlled since cells in the ink are under a certain degree of stress. Thus, studies regarding cell-laden ink extrusion-based freeform 3D printing technologies have focused on enhancing the viability of embedded cells.

Noor et al.[77] reported a novel method to generate customized thick and perfusable cardiac scaffolds with complicated vasculature using induced pluripotent stem cells (iPSCs) with specific differentiating conditions for CMs and ECs (Figure 5). They noted that conventional printing techniques to generate tissues were limited to sizes smaller than whole organs due to the inability to withstand the weight of the printed material. Since the support medium should not harm the laden cells in the objects, biocompatible SA and XG were adopted as the support medium and decellularized omental tissues from humans or pigs were obtained to prepare ink material to contain live cells. The personalized hydrogel utilizing decellularized omental tissue exhibited a nanofibrous structure and its rheological behavior showed a weak state at room temperature but a strong state above 37°C. iPSCs derived from stromal cells in human omental tissues became ECs and CMs after being treated in altered culture medium, and their successful differentiation states were characterized by specific staining methods. Utilizing the abovementioned materials and cells, cardiac patches were fabricated through sequential stacking of CM cell-laden omentum gel, supporting omentum gel, EC-laden gelatin ink, and CM cell-laden omentum gel. The fabricated cardiac patches were incubated at 37°C in order to crosslink the omentum gel and remove the gelatin ink. The feasibility of cardiac patches was demonstrated by transplantation of the patches between rat omentum. Additionally, a much more complex shaped design was created in the supporting bath with comparable cell viability after culturing, printing, and extraction. Eventually, a heart was successfully created with specifically positioned cells to meet the required functions. Although fascinating experimental results were reported, some limitations still exist regarding the efficient use of iPSCs and maturation of the created scaffolds. Similar to the previous approach of selecting 3D printing material, Lee et al.[78] demonstrated the application of composite material consisting of methacryloyl-substituted human recombinant tropoelastin (MeTro) and GelMA bioinks in generating an artificial vascular structure within an easily removable Carbopol bath. They studied the utilization of the abovementioned composite hydrogels in other tissue engineering applications.[89] Lithium phenyl-2,4,6-trimethylbenzoylphosphinate (LAP) was adopted to reduce the harmful effects of UV irradiation, which has conventionally been utilized for photocrosslinking of hydrogels. To generate artificial vasculature, CMs, cardiac fibroblasts (CFs), and HUVECs were embedded into GelMA bioink and HUVECs were embedded into MeTro/GelMA bioink. The prepared bioinks were printed into the Carbopol supporting bath to sustain the vascular structure, and subsequently photo-crosslinked

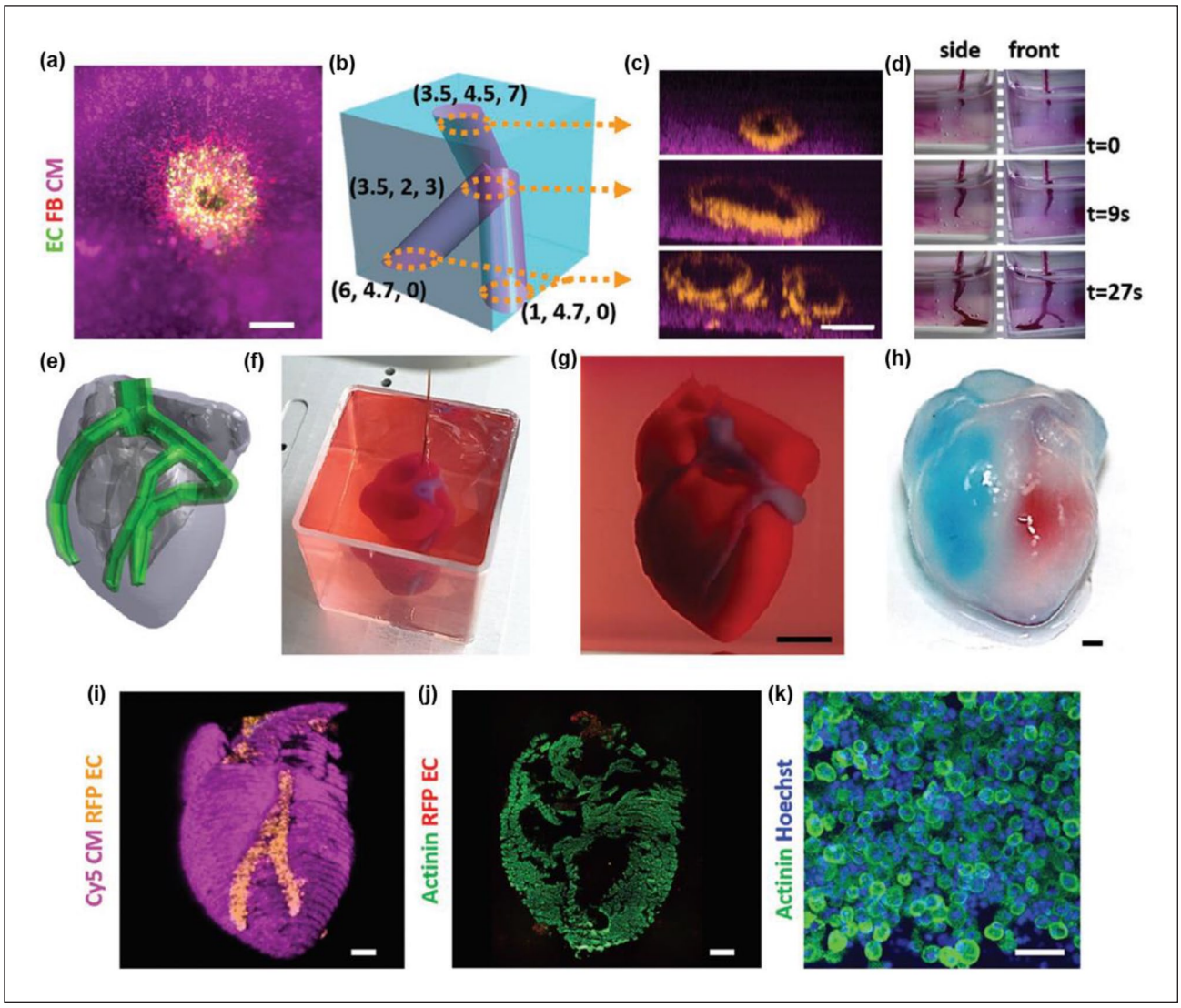

Figure 5. (a) A top view of a lumen entrance (CD31; green) in a thick cardiac tissue (actinin; pink). (b) A model of a tripod blood vessel within a thick engineered cardiac tissue (coordinates in mm). (c) Corresponding lumens in each indicated section of the printed structure. (d) Tissue perfusion visualized from side and front viewpoints. (e) CAD model of human heart. (f and g) A printed heart within a support bath. (h) After infiltration of red and blue dyes into the left and right ventricles of printed heart. (i) 3D confocal image of the printed heart (CMs in pink, ECs in orange). (j and k) Cross-sections of the heart immunostained against sarcomeric actinin (green). Scale bars: (a, c, and h–j) = 1 mm, (g) = 5 mm, and (k) = 50 μm.
Source: Adapted with permission from Noor et al.[77]

with UV light (405 nm). Then, the Carbopol supporting bath was liquefied through immersion in Dulbecco's phosphate-buffered saline (DPBS), allowing the artificial vasculature to be released. The measured diffusional permeability of the cell-laden construct was much lower than that of the acellular construct, and the endothelial barrier function was present in the cell-laden construct. Furthermore, the beating behavior of the CMs incorporated in the vascularized cardiac construct became synchronized between striated muscles as the culturing time increased. In vivo degradation and biocompatibility were evaluated through implantation into subcutaneous rat tissue, and the results exhibited an excellent exchange rate of biomaterial and regenerated tissues with few inflammatory responses. This study demonstrated the complementary effect of GelMA and MeTro using a highly precise 3D printing technique as well as biocompatibility in both in vitro and in vivo tests. However, the fact that the printing procedure of MeTro should be conducted at 8°C due to the material solubility is of concern with respect to cell viability during long-term printing procedures required to generate larger objects.

Another recent study investigated the application of a nanoclay-hydrogel composite supporting bath with sufficient biocompatibility for freeform 3D printing.[79] The study addressed the disadvantages of commonly

used supporting bath materials, such as Carbopol and microparticles, in terms of their sensitivity to the surroundings. Afghah et al. focused on the modification of a sol-gel transition of F127 mixed with Laponite RDS (RDS), which could form a stable polymer-nanoclay complex. They evaluated the effect of the F127 and $CaCl_2$ concentrations on the rheological behavior of F127-RDS. An increase in the F127 concentration increased the storage moduli to a certain range. The storage moduli decreased after that critical concentration, which was increased by the threshold for electrostatic interactions and hydrogen bonding between F127 and RDS. On the other hand, the recoverability of the F127-RDS system in terms of F127 concentration, as determined by dynamic strain tests, demonstrated that a low F127 concentration could not recover the crosslinked chains attached to the RDS. Furthermore, the effect of $CaCl_2$ was also systematically analyzed under constant F127 and RDS concentrations. Similar to the effect of the F127 concentration on rheological behavior, the dynamic moduli of the F127-RDS gels decreased below a certain $CaCl_2$ concentration due to lack of aggregate formation. Based on the results, the final $CaCl_2$ concentration was set to 0.5% as a structural modifier of RDS and cross-linker of alginate for cell-laden ink. Experiments regarding the printability in the F127-RDS supporting bath were conducted by means of creating overhanging structures. Overhanging structures consisting of 20 layers were designed with 90°, 60°, and 45° inclined structures. The printed structure exhibited a similar inclination degree to the initial design, indicating the possibility of fabricating a highly precise structure in the F127-RDS bath without collapse or deformation. Moreover, 3D printing of complicated structures, from star to nose shapes, was proven possible in the supporting bath, and elimination of the supporting bath did not alter the overall structure. Finally, they printed NIH-3T3 fibroblast-laden alginate hydrogel in the supporting bath with a vascular structure (5 mm diameter and 0.6 mm height). During the 7-day cultivation period, the cell viability continuously increased, illustrating that a dramatic change did not occur throughout the printing process. Moreover, they noted that this technique is advantageous for obtaining a final construct from the supporting bath compared to other studies utilizing RDS. Patrício et al.[27] also pointed out the difficulties of using a microparticle-based supporting bath and Carbopol for freeform 3D printing due to the time-consuming process and compatibility of crosslinking agents. Moreover, they commented on the challenges regarding removal of the supporting bath after finalizing the printing process since those methods could affect the viability of cells. As an alternative material for the supporting bath, they introduced XG, whose merit resides in its cost-effectiveness and high pseudo-plasticity. The research investigated two different ways to use XG: as a sacrificial material and as a permanent supporting matrix to retain the vascular structure. A macroscale object larger than 5 cm in length with an asymmetric structure was generated without any gravitational falls in the XG supporting medium, and the embedded structure was well maintained even after removal of the XG matrix. The viscosity of the XG matrix decreased with an increase in shear rate, which resulted in easier extrusion in the matrix and fixation after settling of the printed material. Cells in printed alginate within the XG matrix exhibited a certain degree of viability after they were extracted from the XG matrix and cultured for 7 days. To verify the XG matrix as a biocompatible candidate for cell incorporating material, XG was modified with a methacrylate functional group (XG-GMA) and fibroblasts were added into the hydrogel matrix. Alginate was printed along the XG-GMA matrix to generate a channeled structure and was then removed by perfusion. Even after the perfusion, the cells were viable in the XG-GMA matrix compared to the bulk hydrogel, which contained large amounts of dead cells after 7 days of culturing. The perfused channels (within 350 μm) were surrounded by live fibroblasts and the structures were maintained. Through a series of experiments, they demonstrated the versatility of XG hydrogel as a supporting and biocompatible material for freeform 3D printing.

Cell construct-based freeform 3D printing technologies

Material and cell-laden ink extrusion-based freeform 3D printing technologies have achieved highly advanced results utilizing various candidates for biocompatible inks within versatile supporting matrices. However, there remain concerns about the harmful effects of the remaining polymer residues in the matrices and the use of additional crosslinking agents. Thus, recent investigations have focused on utilizing cell constructs, including MCSs or cellular organoids, as an original printing material with a greatly reduced amount of additional matrix to sustain cell viability.

MCSs were utilized as a raw printing source to generate vascular constructs by Norotte et al.[80] The article proposed scaffold-free vascular tissue engineering techniques through fabrication and printing of cellular spheroids containing Chinese Hamster Ovary cells, HUVSMCs, and HSFs. Agarose rods were initially deposited to support the printed cellular spheroids, and the designed tubular structure was fully covered with agarose rods. Complex tubular structures with different sizes and aspect ratios could be created by controlling the number of agarose rods entrapped in the rods of cellular spheroids. Furthermore, a branched structure with distinct channel sizes was also generated by intercrossing agarose rods. Fully automatic printing was possible since the equipped syringes containing agarose and cellular spheroids followed an identical printing path. Printed MSCs required fusing for 2–4 days to stabilize the structure before removal of the agarose

rods, and double-layered vascular tubes were fabricated using HUVSMC and HSF spheroids, which mimic the media and adventitia of macrovasculature. Interestingly, alternatively positioned cellular spheroids resulted in an exceptional structure that could not be observed in nature. In histological examinations, complex vasculatures were successfully manufactured after 3 days of fusion. Thus, this research presented the possibility of fabricating complex and customized vascular constructs by patterning cells without scaffolds.

Another recent article reported the use of iPSCs in the form of organoids that acted as a supporting bath for a vascular construct (Figure 6).[82] They designated the technology as sacrificial writing into functional tissue (SWIFT) composed of a living organ building block (OBB) matrix. The OBBs were composed of embryoid bodies (EBs), organoids, or MSCs based on iPSCs. Cell aggregates were prepared through compulsive partitions using microwell array plates. The microwell array plates were specifically designed as inverted pyramid structures and were produced by PDMS molding. Separated cells started to aggregate into EBs or spheroids, which were cultured to gather massive amounts of cell aggregates. The obtained aggregates were untangled into an ECM-based solution containing collagen I and Matrigel, and the prepared matrix was centrifuged to acquire a densified matrix on which sacrificial ink would be printed. Gelatin was used as a sacrificial ink and it was dispensed through a metal nozzle with an inner diameter of 0.25 mm. The printing of sacrificial gelatin ink was conducted at 0°C–4°C, at which temperature gelatin maintains a gel-like state. Subsequently, whole structures were heated to 37°C to induce gelation of the ECM solution and melt the gelatin ink. Finally, molten gelatin sacrificial ink was perfused using a peristaltic pump to evacuate the channeled structure in the matrix. Additionally, supplemented iPSCs were specifically differentiated into cerebral organoids and cardiac spheroids using certain environmental conditions to exhibit the utility of iPSC-laden OBB matrices. Channeled structures were well maintained after evacuation of the sacrificial ink and the viability of cells was retained. A monolayer of HUVEC endothelium was formed in the EB matrix by filling HUVECs into the readily perfused channel. Notably, a freeform vascular channel was generated in the cardiac tissue matrix following SWIFT, and the tissue presented an intrinsic ability to alter the beating behavior following external electrical pacing and administration of isoproterenol (a nonselective agonist for the β-adrenoreceptor) and heptanol (a gap junction blocker).

Diverse methods for differentiating iPSCs were further utilized to generate vascularized organoids by orthogonal differentiation.[81] Human induced pluripotent stem cells (hiPSCs) were exposed to different cell types through restrained culturing conditions. This study used one wile type (WT) line and two inducible-transcription factor (TF) lines from the Personal Genome Project 1 (PGP1) hiPSC lines as starting cell lines. WT PGP1 cells cultured in neural induction medium (NIM) transformed into neural stem cells. Doxycycline-induced ETV2 isoform-2 overexpression and doxycycline-induced NGN1 overexpression of inducible-TF lines resulted in the formation of inducible endothelial (iEndo) cells and inducible neurons (iNeurons), respectively. After confirmation of the differentiating behavior, the possibility of heterogeneous differentiation was examined. Different portions of WT, iEndo, and iNeuron were cultured on the Matrigel surface with doxycycline supplemented NIM. After 6 days of culturing, iEndo formed a microvasculature, iNeuron formed a network of neurites, while WT formed neurospheres. In addition, they initially tried to resolve the difficulties of organoid vascularization in microwells using simple mixing of ECs and hiPSCs. However, this simple mixing resulted in phase separation because of the different mechanisms for cell adhesion. As a solution for this issue, the WT+ iEndo ratio was adjusted for precise tailoring of the resulting endothelium. Comparing WT-only organoids and WT+ iEndo organoids after culturing, only WT+ iEndo groups exhibited developed vascularized cortical organoids and ventricle-like architectures, illustrating a promoted vascular network formation. In addition, they combined WT, iEndo, and iNeuron cells to resemble a developing brain consisting of a germinal zone, surrounding neurons, and perineural vascular plexus. Organoids with a radial-symmetric multicore-shell structure were successfully produced by V-shaped wells. Eventually, direct printing of pluripotent inks in a gelatin-fibrinogen ECM was conducted with considerably high cellular density. Individually printed WT, iEndo, and iNeuron filaments formed neurectoderm filaments, a microvascular network, and a pervasive network of neurites after culturing. Three of the bioinks were simultaneously printed through a multi-material print head with an inner diameter of 250 μm. Treatment of the printed construct with doxycycline induced simultaneous orthogonal differentiation of the contained cells in a layered structure. Layered structures containing orthogonally differentiated cells were well fabricated by multi-material 3D bioprinting, including programmable cellular organoids, which would provide a useful platform for examination of therapeutic agents before in vivo and clinical tests.

Photodegradation-based freeform 3D printing technologies

High-energy lasers have been utilized in numerous fields for selective carving of certain materials to generate personalized patterns. In tissue engineering, researchers have noticed the usefulness of lasers to create voids in soft materials. Additionally, by controlling the continuous path of focus based on a predetermined design, complex shaped structures can be fabricated. This subtractive strategy

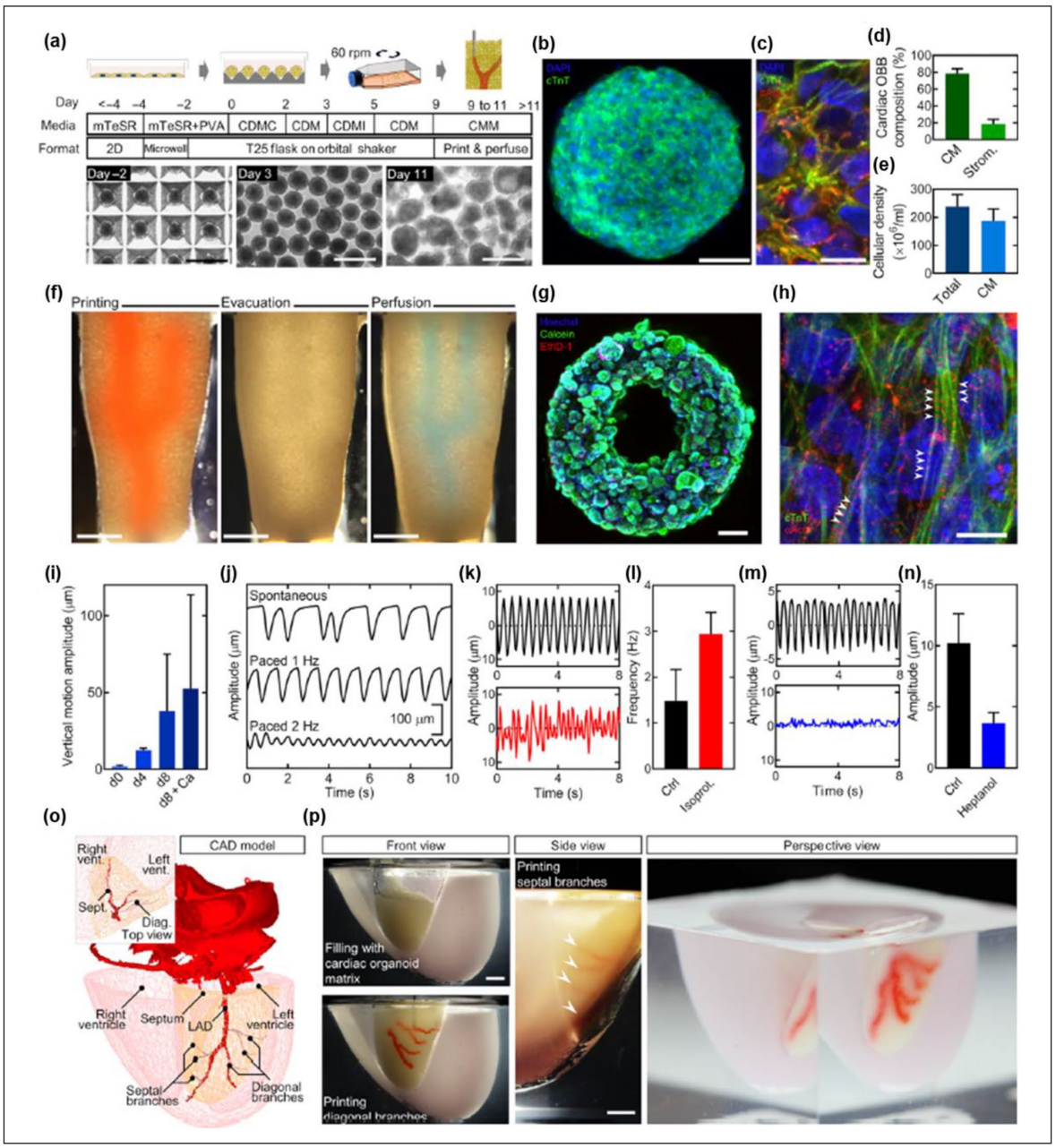

Figure 6. (a) Differential protocol of cardiac organoid. (b) Cardiac troponin T and 4′,6-diamidino-2-phenylindole (DAPI) staining in a single cardiac OBB at day 9. (c) Cardiac troponin T, α-actinin, and DAPI staining in a single cardiac OBB at day 9. (d) Cardiac spheroid composition in iPSC-derived cardiac OBB. Identified CMs (CM) and stromal-like cells (strom.) by cardiac troponin T-positive ($cTnT^+$) and $cTnT^-$/$Vimentin^+$, respectively. (e) Cellular density in compacted cardiac OBB tissue. (f) An image sequence showing the embedding, evacuation, and perfusion of branched vascular channels within a cardiac tissue matrix (tissue dimensions: top width, 6 mm; bottom width, 4.2 mm; depth, 4.2 mm; and height, 12 mm). (g) Viability staining of a SWIFT cardiac tissue (cross section) after 24 h of perfusion. (h) Evidence of sarcomeric remodeling through cTnT, α-actinin, and DAPI staining in a SWIFT cardiac tissue after 8 days of perfusion (arrowheads). (i) Increasing vertical displacement of the anchoring flexible prongs over time due to spontaneous CM contraction. Two millimolar calcium was added to the medium to increase CM contractility ("d8 + Ca") on day 8. (j) Comparison of anchor displacement pattern between spontaneous contraction and electrical pacing (1 and 2 Hz) of SWIFT cardiac tissues. (k) Spontaneous contraction pattern before and after administration of 10 μM isoproterenol. (l) Average contraction frequency under isoproterenol treatment. (m) Spontaneous contraction pattern before and after administration of 1 mM 1-heptanol. (n) Maximum peak-to-peak contraction amplitude under 1-heptanol treatment. (o) 3D CAD model of a normal human heart including a segment of the left anterior descending (LAD) artery and a diagonal branch. (p) A 1:2 scale polydimethylsiloxane mold fabricated by the 3D computed tomography data and the LAD artery together with diagonal and septal (arrowheads) branches embedded into a septal-anterior wall wedge (yellow section in (o)) of the cardiac tissue matrix via SWIFT. Scale bars: (b) = 50 μm, (c and h) = 10 μm, (f) = 2 mm, (g) = 500 μm, and (p) = 5 mm.
Source: Adapted with permission from Skylar-Scott et al.[82]

using lasers, which is absent of cytotoxic agents and extensive labor, has been investigated to generate freeform vascular structures in hydrogels.

Applegate et al.[83] reported the utilization of lasers to produce a 3D multiscale micropatterned structure in biocompatible hydrogel. This research adopted multiphoton adsorption (MPA) of light using highly transparent elastomeric SF hydrogel as a photodegradable hydrogel that could maintain internal voids formed following movement of the laser focus. SF hydrogel is suitable for this application due to its transparency (which is related to laser penetration), stiffness associated with structural integrity, and biocompatibility for tissue engineering. The power of the laser was optimized at sub-2 nJ per pulse, 810 nm wavelength, and 80 MHz repetition rate. Specifically, they could form voids 1 cm below the top of the hydrogel, which is the deepest among related studies. The effect of the pulse energy on the void size was evaluated using pulses with 0.25–5 nJ of energy. Increasing the pulse energy from 0.25 to 5 nJ resulted in an increase in full width at half maximum and depth of trench. Representative complicated structures (i.e. helix and vessel-like structures) were micromachined into the silk gel, and traces of material removal were shown in the edges of the machined parts. The biocompatibility of the machined gel parts was confirmed by culturing human foreskin fibroblasts on the surface of the linearly micromachined hydrogel. The cells tended to grow following the grooves, which corresponded to cell alignment. To demonstrate the applicability of this multiphoton micromachining technique to tissue engineering, a 3D branched structure was formed in the silk hydrogel and the culture medium containing live cells was infiltrated into the channels. The number of attached cells found in the bottom parts of the branched channels increased with prolonged culturing time. Additionally, a preliminary in vivo study was performed by implanting the micromachined gel in mice. Similar to the results of the in vitro cell infiltration test, the cell density was higher in the bottom part of the branched structure compared to the top part, which was driven by the migration of cells. Although this study focused on the utilization of silk hydrogel, other hydrogels containing photolabile bonds could be used for multiphoton micromachining.

The use of focalized laser pulses to fabricate highly controlled microfluidic networks in hydrogels was also reported by Brandenberg and Lutolf (Figure 7).[84] They used a nanosecond-pulsed laser of a micro-dissection microscope to create microfluidic channels in hydrogel contained in PDMS mounts. The stability of the generated channels in the hydrogel was examined using perfusion, and the channels were maintained for 48 h regardless of flow. Notably, one of the advantages of this technique is the possible extension of readily made channels following the desired structure. A source-sink system, which is a physiological gradient system, was constructed and evaluation of the diffusion using FITC-Dextran and maleimide-Alexa-546 verified the stability of the gradient system. As a cell-encapsulating system, the viability of C_2C_{12} cells (Mouse Myoblast cell line) after the ablation of hydrogel was demonstrated to be comparable to that in a standard culture system. Noting the key roles of MSCs in tissue dynamics, the directional migration of MSCs following chemoattractant platelet derived growth factor-BB (PDGF-BB) was also evaluated. A short pulse of PDFG-BB induced migration of MSCs into the PEG hydrogel. Other than biocompatible PEG hydrogel, collagen type I-based hydrogel was also adopted as a basic material to be carved by laser. After producing a channel structure in the collagen type I-based hydrogel, HUVECs were seeded in the channel to illustrate vascular application of this technique. After 5 days of culturing, densely packed HUVECs following the hydrogel channel were detected by immunostaining endothelial markers. Due to the simple and user independent laser etching technique, fabrication of microfluidic networks in the hydrogel was easily accomplished. The sterility of the cell culture was guaranteed since the source of degradation is light, and creation of the customized channel structure was possible by controlling the movement of the laser.

The importance of vascularity in organ systems, in terms of transporting nutrients, electrolytes, and cells, provoked the modification of hydrogel materials to be more biocompatible and photodegradable.[85] Arakawa et al. designed photodegradable hydrogels by azide-alkyne cycloaddition (SPAAC) between poly(ethylene glycol) tetrabicyclononyne (PEG-tetraBCN, Mn ≈ 20,000 Da) and a diazide-functionalized synthetic peptide [N3-oNB-RGPQGIWGQGRGDSGK(N3)-NH2]. The RGDS moieties contained in the synthetic peptide have been known to promote cellular responses. All of the materials, including the synthetic peptides, were crosslinked through step-growth polymerization. The incorporated ortho-nitrobenzyl ester (oNB) moiety could be degraded by pulsed near infrared light. As a degrading technique, multiphoton lithography was applied, which can produce precisely controlled submicrometer-scale 3D structures in the hydrogel. Channel networks were fabricated by perfusing the degraded hydrogel, and the dimensions were varied from 200 μm × 200 μm to as small as 10 μm × 10 μm. The connectivity between the channels was demonstrated by perfusing fluorescent beads into the lumens. Biomimetic perfusion using fluorescent beads with diameters of 2 μm (similar to platelets) was carried out and the beads were found through iterative photodegradation. Using cell capture devices, microtraps within the hydrogel networks were also intended. To illustrate the creation of vascular networks, HUVECs were perfused into the photodegraded fluorescein-modified PEG hydrogels. HUVECs were seeded onto the channels with dimensions from 100 μm × 100 μm to 45 μm × 45 μm. The HUVECs

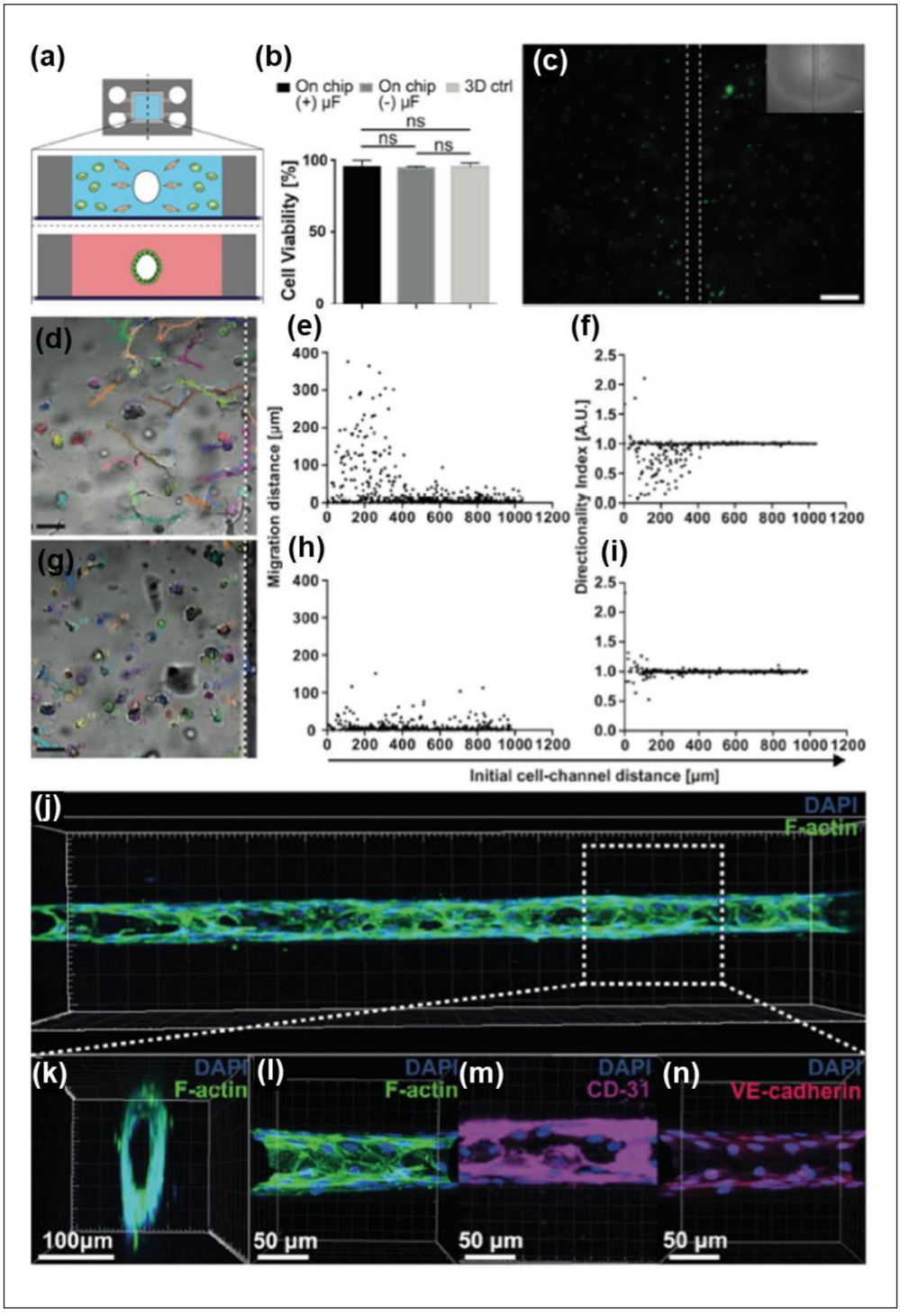

Figure 7. (a) Schematic representation of the two in vitro models (3D invasion assays and blood vessel-like structures) generated by laser-based fabrication of biomicrofluidic networks in hydrogels. (b) Assessed cell viability by live/dead staining (green: live cells, red: dead cells) with 1 h after the fabrication process (3D ctrl: conventional 3D culture on a 24-well plate, (−) µF and (+) µF: PDMS mounts without and with the fabricated network). (c) Wide-field fluorescent image of a representative, live/dead stained mouse myoblast (C_2C_{12}) culture. (d) A representative bright-field image overlapped with the cell tracks of prestarved hMSCs perfused with PDGF-BB for 30 min. (e) Analysis of the migration distance and (f) the directionality index of hMSCs perfused with PDGF-BB for 30 min. (g) Representative bright-field image overlapped with the cell tracks of prestarved hMSCs perfused with medium only. (h) Analysis of the migration distance and (i) the directionality index of hMSCs perfused with medium only. (j) Confocal 3D reconstruction of a hollow HUVEC tube formed in collagen type I. (k) Transversal and (l) frontal plane of the structure. Frontal planes showing endothelial markers immunostainings of (m) CD-31 and (n) VE-cadherin.
Source: Adapted with permission from Brandenberg and Lutolf.[84]

attached and spread on the surroundings of the hydrogel without any sign of cytotoxicity. Furthermore, the cytocompatibility of the photodegradation method was assessed by generating channels in human bone marrow-derived hS5 stromal cell-laden hydrogel and perfusion of HUVECs. After 4 days of culturing, human bone marrow-derived hS5 stromal cells around the photodegraded parts were still alive while HUVECs covered the outer layer of the channel. Although an excellent system for generating freeform vascular structures was developed, several limitations exist, such as penetration depth, speed, and effectiveness, which still need improvement.

Projection stereolithography-based freeform 3D printing technologies

Although great achievements have been made in generating artificial constructs by versatile 3D printing techniques, there have been some limitations regarding the resolution of the printed scaffolds, efficiency of the technique, and viability of laden cells. Compared to the extrusion-based 3D printing technique, which is the most prevalent technique in the field, the projection stereolithography technique is free from external extrusion forces that apply additional stress to viable cells. This technique is widely utilized to create highly delicate structures using photopolymerizable polymers. However, the fact that the photopolymerization mechanism is identical to photocrosslinking of several hydrogel systems has led to the application of projection lithography for fabrication of artificial vasculatures in hydrogel systems.

DLP-based microscale continuous optical bioprinting (μCOB) was adopted to create pre-vascularized tissue constructs in supporting hydrogel with high speed and resolution.[86] Since the designed structure must be maintained following photocrosslinking in hydrogel, the basic materials should be photocrosslinkable and biocompatible. Thus, the research utilized glycidal methacrylate-hyaluronic acid (GM-HA) and GelMA mixed with synthesized LAP in which the designed construct would be produced. GM-HA and GelMA were used in the research due to their ability to be photopolymerized and their excellent biocompatibility even after methacrylate modification. Different prepolymer solutions consisting of GM-HA, GelMA, LAP, and cells were stacked LbL. After the non-prevascularized prepolymer solution was cured for the supporting layer, the prevascularized prepolymer solution (cell-laden prepolymer solution) was cured in the channeled structure. Subsequently, the non-prevascularized prepolymer solution was applied to cover the vascular constructs. Channeled structures with uniform and gradient widths were generated using HUVECs in liver hepatocellular cell (HepG2)-laden hydrogel. A complicated channeled structure with diameters varying from 5 to 50 μm was successfully generated due to the advantage of μCOB, and the different mechanical properties between the channel and supporting parts were expected to induce lining of the cells in the channels. To create a hollow structure in the GelMA matrix, GM-HA was degraded using hyaluronidase (100 U/mL), which resulted in the removal of hydrogel within 48 h. In vitro tests using HUVECs and mesenchymal cells (10T1/2) for the formation of a channel structure in the hydrogel were also carried out with 1 week of culturing. After culturing, the construct was stained with a fluorescent cell tracker and human-specific CD31, which demonstrated a connective network between the HUVECs in the channels. In vivo experiments conducted using subcutaneous implantation into mice revealed that the non-prevascularized tissue construct was preserved after a 2-week follow-up period. Particularly for the prevascularized tissues, a significantly higher degree of vascular area density and average vessel counts were observed compared to those from the non-prevascularized tissues, indicating successful anastomosis of the implanted tissues to the host tissues.

Stereolithography apparatus for tissue engineering (SLATE), which is an emerging technique for 3D freeform fabrication, was utilized to create multivascular networks within a biocompatible hydrogel (Figure 8).[87] The research first focused on finding an appropriate nontoxic light absorber to obtain high precision in a water and PEGDA system. Tartrazine, curcumin, anthocyanin, and gold nanoparticles were examined in terms of absorbance spectra and modulus. Among those candidates, tartrazine was chosen as an appropriate photoabsorber because of its low toxicity, hydrophilicity for easy rinsing, transmittance, and possible degradability during photopolymerization. Using the mixture of water, PEGDA, LAP, and tartrazine, a chaotic mixer was constructed to homogenize fluids in vessels. An enhanced mixing ratio was observed by increasing the number of fins in the mixer. Hydrogels with a 3D bicuspid valve were fabricated, and the valve leaflets reacted to pulsatile anterograde and retrograde flows. A helix surrounding an axial vessel, 1° and 2° Hilbert curves, a bicontinuous cubic lattice (based on a Schwarz P surface), and a torus entangled with a torus knot were fabricated as a demonstration of vascular networks. A tessellation structure was created with a central path through which gas penetrated, and a channel through which deoxygenated red blood cells (RBCs) moved. Dark red colored deoxygenated RBCs became bright red as they passed by the central path, which had a higher concentration of oxygen. Moreover, an alveolar model topology was printed based on Weaire–Phelan 3D tessellation. Differently positioned airways and vasculatures were generated and tidal ventilation was applied to the airways. Notably, expansion of the airways interrupted the flow of RBCs, which resulted in RBC clearance. 3D computational model analysis also supported the results that anisotropic swelling occurred during inflation of the air sac.

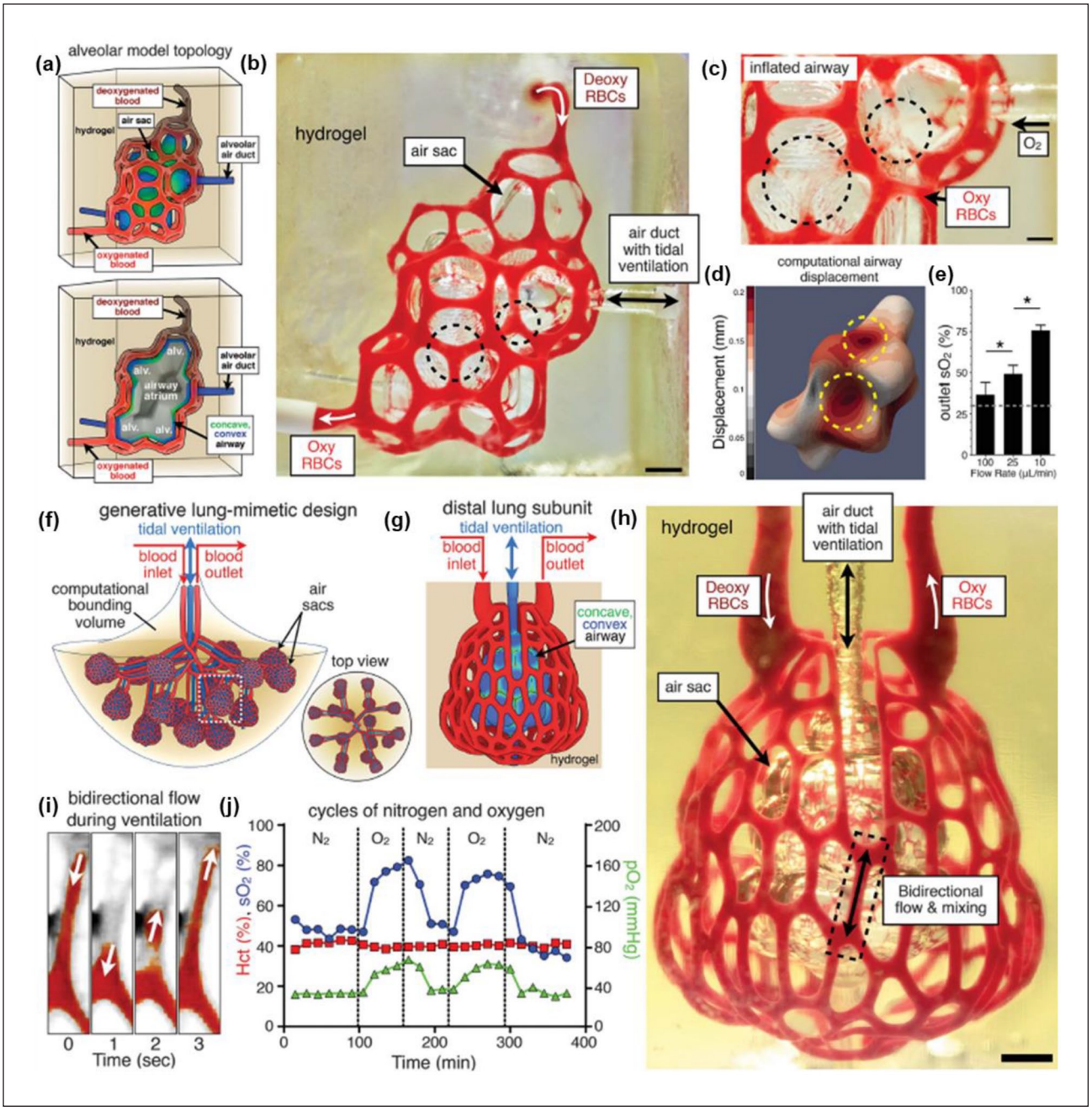

Figure 8. (a) (Top) Architectural design of an alveolar model topology based on a Weaire-Phelan 3D tessellation and topologic offset to derive an ensheathing vasculature. (Bottom) Vertical cross-section of the model alveoli (alv.) with a shared airway atrium (blue: convex regions of the airway, green: concave regions of the airway). (b) Photograph of a printed hydrogel during RBC perfusion during ventilation of air sac with O_2. (c) RBC clearance and squeezed blood vessels by concave regions of the airway (dashed black circles) upon airway inflation with oxygen. (d) A computational model of airway inflation presenting increased displacement at concave regions (dashed yellow circles). (e) Increased oxygen saturation of RBCs following decrease in RBC flow rate ($N = 3$, $^*p < 9 \times 10^{-4}$ by Student's t-test). The dashed line indicates sO_2 of deoxygenated RBCs perfused at the inlet. (f) Diagram of a lung-mimetic design through generative growth of the airway, offset growth of opposing inlet and outlet vascular networks, and population of branch tips with a distal lung subunit. (g) The distal lung subunit composed of a concave and convex airway ensheathed in vasculature by 3D offset and anisotropic Voronoi tessellation. (h) Photograph of a printed hydrogel containing the distal lung subunit during RBC perfusion while ventilation of air sac with O_2. (i) Bidirectional RBC flow during ventilation represented by threshold view of the area enclosed by the dashed box in (h). (j) Ability to withstand ventilation for more than 10,000 cycles (24 kPa, 0.5 Hz) of distal lung subunit and illustration of RBC sensitivity to ventilation gas (N_2 or O_2). Scale bars : (b and h) = 1 mm and (c) = 500 μm.

Source: Adapted with permission from Grigoryan et al.[87]

Extended work was performed to construct a lung-mimetic design with a fixed vasculature inlet and outlet and an air duct. During the inflow and outflow of the RBCs through the vasculature, deoxygenated RBCs became oxygenated after humidified oxygen was infiltrated through the air duct. The partial pressure of oxygen (pO_2) and oxygen saturation (sO_2) fluctuated following the cycle of N_2 and O_2, while hematocrit (Hct) was maintained under more than 10^4 ventilation cycles. In vivo examination using bioprinted hydrogel carriers containing hepatocytes was carried out by suturing them to the perigonadal fat pad of mice. After implantation, the albumin promoter activity was maintained considerably higher in hepatic hydrogel carriers compared to tissues containing single cells. Additionally, an advanced carrier containing hepatic aggregates and ECs was implanted in mice with chronic liver injury. After 14 days of implantation, implication of surviving functional hepatocytes was noted and hepatic aggregates adhered to the hydrogel were observed through immunohistological assessment. These results demonstrated the possibility of solving long lasting design limitations.

In terms of photopolymerizable ink for vascular applications, degradability under physiological conditions is a necessary aspect. Thomas et al.[88] explored degradable bioink systems that could be utilized for vascular printing through projection-based SLA. They addressed the strategy to adjust the degradation kinetics for rapid release of incorporated ECs, which would eventually construct artificial vessels. To achieve that, three different materials, GelMA, methacrylated hyaluronic acid (HAMA) with reduced chain length, and acrylated hyaluronic acid (HAA), were used to find the appropriate concentration for vascular printing. Systematic characterizations of Young's modulus and viscosity proved that the use of HAA induced higher viscosity compared to HAMA. Thus, HAMA-containing groups were further tested for swelling and degradability. The swelling ratio of differently proportioned HAMA and GelMA hydrogels exhibited HAMA concentration dependent behavior, while degradability was greatly affected by the GelMA component. Based on the obtained mechanical properties and degradability results, 1.5% HAMA solution was chosen as a bioink for vascular printing. The viability of HUVECs incorporated in the HAMA hydrogel was examined by immersion in different concentrations of hyaluronidase (Hase) solutions. Interestingly, the viability of HUVECs in the absence of Hase was significantly reduced compared to hydrogel containing Hase. This suggests that cells embedded in the hydrogel system should rapidly escape the matrix to avoid apoptosis. For vascular bioprinting, the permanent supporting matrix was composed of GelMA and LAP, and the channel matrix was composed of HAMA and LAP. Endothelial cell-laden HAMA hydrogel was printed into the GelMA matrix, and the entire construct was immersed in the medium for 28 days. Two-photon microscopy revealed printed and released HUVECs attached to the GelMA matrix walls that had proliferated within the vascular construct.

Challenges

Despite the recent progress in freeform 3D printing systems, there are still several challenges that must be addressed to make this approach more acceptable for fabrication of vascularized artificial tissues as shown in Figure 9. Currently, these include, but are not limited to, strain field effect, nozzle translating speed, and cross-sectional shape control issues.

Effect of strain fields around the printing nozzle

As the supporting matrix plays the role of holding the printed inks and minimizing ink displacement during the printing process, the structural resolution of the printed object is largely influenced by the mechanical properties of the supporting matrix: shear elastic modulus (G') and yield stress (τ_y).[25,35] Qualitatively, if the G' of the supporting matrix is lower than that of the printing ink, dragging of the extruded printing ink can occur followed by translation of the printing nozzle, thereby leading to substantial spatial deviation from the intended position.[35] In addition, when τ_y of the supporting matrix is lower than the viscous stresses associated with displacement of the printing nozzle, the translating nozzle creates stress fields that yield and displace the printed features.[25,90] However, at the same time, as τ_y of the supporting matrix should be low enough to allow the translating nozzle to move freely throughout the supporting matrix, there is a practical upper limit of the τ_y of the supporting matrix, and a greater or lesser displacement of printing structures from the intended form are inevitable. Grosskopf et al.[35] revealed how matrix yielding impacts their fidelity. By analyzing the crossover point of G' (shear elastic modulus) and G'' (viscous modulus) using shear rheometer tests, they identified the τ_y of a PDMS supporting matrix, and with the content of fumed silica particles increasing from 33 to 66 wt%, its τ_y largely increased from 1.3 ± 3 to 48.2 ± 6 Pa. From a practical 3D printing test using F127 ink, the supporting matrix with low τ_y exhibited a pronounced deviation from the intended form, while printing in the supporting matrix with high τ_y most closely followed the intended form. However, in the case of the PDMS supporting matrix with the highest τ_y, there were still noticeable discontinuities at the junction of the two printing segments. When the nozzle was translated away from the junction where neighboring segments were printed, strain fields near the printing nozzle in the supporting matrix caused the deposited ink to be dragged or shifted, and the junction was slightly off center.

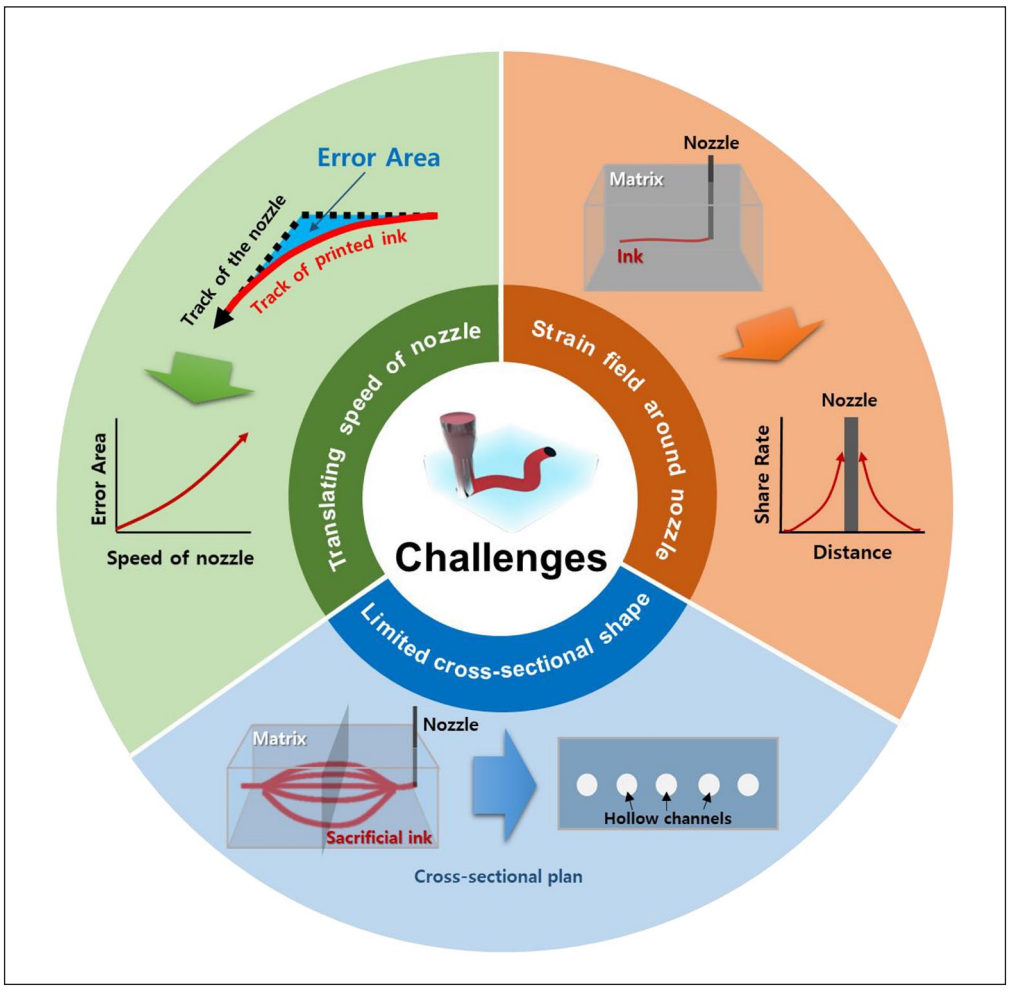

Figure 9. Challenges of freeform 3D printing for fabricating artificial tissues with vascular structures.

To minimize the dimensions of the yielded regions around the nozzle during freeform 3D printing, the Oldroyd number (*Od*) is a useful parameter, especially in the supporting matrix following the Herschel–Bulkley equation. The *Od* generally represents the ratio of material τ_y to the viscous stresses in the flow and can be expressed as follows:

$$\text{Oldroyd number } (Od) = \frac{\tau_y d^n}{KU^n} \quad (1)$$

where τ_y, K, and n are given by the Hershel–Bulkley equation, d is the outer diameter of the cylindrical printing nozzle, and U is the speed of the translating nozzle.[35,91,92] From the quantitative analysis, when $Od < 1$, the width of the yielded region around the nozzle changes rapidly with changes in the *Od*, while when $Od > 1$, the width changes less with changes in the *Od*. In addition, it was confirmed that the print fidelity increases with increasing *Od* values under the predetermined printing path and conditions (nozzle diameter, translating speed, and flow rate). However, with $Od > 1$, the supporting matrix was too stiff to allow the printing nozzle to move without developing crevices behind the translating nozzle due to its slow recovery time.[35] Therefore, there is still a strong requirement for the development of suitable matrix materials for freeform 3D printing that possess a high *Od* value as well as thixotropic behavior that allows the matrix to "self-heal" during the printing process.

Limitation of high translating speed of printing nozzle

In freeform 3D printing, the printing speed directly affects the total printing time of the 3D printed parts as well as the quality of the line and width of the printed ink in the supporting matrix. As the translating velocity of the printing nozzle increases, the extruded printing ink experiences some tensional stress at the interface between the ink and supporting matrix and becomes thinner.[93] However, the printing speed is also a significant parameter affecting the

dimensions of the yielded regions in the supporting matrix around the printing nozzle.[25,35] As described by equation (1) in section "Effect of strain fields around the printing nozzle," the *Od* is inversely proportional to the speed of the translating nozzle, and a lower *Od* value leads to larger non-dimensional yielded regions in front of and behind the nozzle, eventually leading to pronounced deviation from the intended shape. Uchida et al.[93] also evaluated the effect of nozzle translating speed on the accuracy of the printed patterns by defining the error area of freeform 3D printing as the dragged area of the printed ink at the corner region with an angle of 30°, 60°, 90°, 120°, or 150°. Although the freeform 3D printed structures was significantly influenced by the angle of the corner, faster nozzle translating speeds led to higher error areas for all printing angles.

In the case of the supporting matrix with thixotropic behavior, its time-dependent change in viscosity property allows a time scale for the supporting matrix recovery after removing the applied stress by translating the printing nozzle.[94,95] Ideally, for successful freeform 3D printing, reflow of the supporting matrix should occur immediately after nozzle translation, so that the printed ink can be stably trapped in the designed position and shape inside the supporting matrix. However, most thixotropic matrix materials require a certain time duration for restructuring; hence, when the printing nozzle is translated with high speed, crevices develop behind the nozzle, which take a much longer time to be filled through dynamic restructuring of the supporting matrix during freeform 3D printing.[96,97] To prevent dynamic crevice formation, the printing speed should be set according to the following relationship:

$$\nu < \frac{\rho g L}{\eta} \tag{2}$$

where ν and L are the translating speed and submerged depth of the printing nozzle, respectively, g is the gravitational acceleration, and ρ and η are the density and viscosity of the supporting matrix, respectively.[25] Therefore, to print 3D structures containing corners with a certain angle and using thixotropic supporting matrices, it is necessary to apply a slow nozzle translating speed to enhance the accuracy of the freeform 3D printed structures, which would be problematic for printing a full-scale vascularized organ because it would take too long to print.

Difficulty in controlling the cross-sectional shape of the printed hollow channels

Another challenge of freeform 3D printing is the difficulty in controlling the cross-sectional shape of the hollow vascular channels within the supporting matrix. Although human blood vessels usually have a rounded cross-sectional shape and generate axis-symmetrical blood flow and uniform shear stress distribution, morphologically different types of blood vessels are also reported in the human body.[98,99] For example, by compressing tumor vessels and changing their cross-sectional shape, Padera et al.[100] showed that cross-sectional shape abnormalities of blood vessels were more common around cancer cells, which leads to an obstacle for the delivery of therapeutic drugs into tumors. Similarly, Goel et al.[101] described that the blood vessels in tumors exhibited triangular cross-sectional shapes with sharp corners where angiogenic processes were significant.

In freeform 3D printing, the printing ink rheology, support rheology, and surface tension between the ink and supporting matrix are known to affect the morphology of the ink extruded into the supporting matrix.[25,35] However, so far the variations are insignificant and almost negligible, showing merely rounded cross-sectional geometries. From the simulated investigation by Friedrich et al.[90] using Newtonian and Herschel–Bulkley inks and supporting matrices, when Herschel–Bulkley fluids were included, the cross-sectional shape of filaments changed from circular to rounded oval shapes as defined by yielding, whereas when Newtonian fluids were included, it was defined by a balance between viscous dissipation and interfacial tension. With a Newtonian supporting matrix at high viscosities, most 3D printed filaments exhibited oval shaped cross-sections with a sharp edge at the top of the filament, and with decreasing viscosity of the ink, the filaments were more elongated vertically and the top of the filament became taller. In contrast, when the viscosity of the ink was high enough to the solid–liquid transition of the Herschel–Bulkley supporting matrix, most printed filaments showed rounder cross-sections, whereas with decreasing ink viscosity, the ink formed laterally wide cross-sections with sharp edges on both sides of the filaments. Although both the Newtonian and Herschel–Bulkley supporting matrices produced accurate positioning of freeform 3D printed filaments, there were minor differences in the cross-sectional morphology of the filaments.

Other issues

The difficulties in printing artificial tissues with vascularized structures can potentially be addressed by negative freeform 3D printing, in which a sacrificial ink is used to print an internal vascular structure, and after solidification of the supporting matrix, it is removed to create hollow vascular channels.[25,82] Because most biomaterials are hydrophilic, negative freeform 3D printing studies have generally used hydrophilic sacrificial inks and supporting matrices. Thus, the printed sacrificial ink becomes narrower and gradually disappears with time due to its diffusion in the supporting matrix.[90,93] This phenomenon would be a problem for printing small-diameter vascularized structures, such as a capillary vessel with a 5–10 μm diameter, or a full-scale functional vascularized organ that takes longer to print.[102]

Biocompatibility of the freeform 3D printing materials is another concern. Although the major elements of the freeform 3D printing ink and supporting matrix are nontoxic, other compositions or experimental processes may adversely affect cells.[103] For example, it is necessary to polymerize the printed ink or supporting matrix immediately after the freeform 3D printing, and photocrosslinkable hydrogels have been most widely used for the encapsulation of cells. However, cell viability of photocrosslinked hydrogels may be adversely affected by photoinitiators and UV exposure.[103,104] Biocompatible photoinitiators and UV-curable polymers are being developed, but most of these studies are still in progress.

Future outlook and conclusion

Vascularized structures in tissue-engineered constructs such as 3D printed artificial organs are essential for the supply of nutrients and oxygen and removal of living cell waste. In particular, for tissues demanding a high level of oxygen, such as the heart, applicable vascularization is of great importance in the body after implantation. Although 3D printing technologies contribute to the biofabrication of vascular networks, a bottleneck remains in the 3D printing of perfusable tubular structures that behave like native blood vessels.

Native organs with blood vessels are complex tissues composed of specific cells and proteins, thus it is difficult to design printable bioinks to fabricate 3D printed artificial organs. Recently, machine learning has become an alternative to solve this problem. The printability of a bioink for artificial organs is generally determined by its shape accuracy, resolution, and biocompatibility. Moreover, as the type of bioink changes, 3D printing parameters, such as printing speed, pressure, and movement distance, also must be adjusted to construct elaborate structures. The main goal of machine learning is to predict the optimal conditions for 3D printing, and design the optimal composition of bioinks to 3D-print the vascular structure. A universal relationship between the printability and mechanical properties of bioink was established by Lee et al.[105] based on machine learning. They found various bioink formulations that provide high printing accuracy with high cell viability after 3D printing. More recently, Ruberu et al.[106] established the optimal printing conditions and optimal ratio of GelMA and HAMA bioinks. Although there remains much to study in this field, it is certain that machine learning is a promising process for constructing vascularized structures.

Nonetheless, it is difficult to fabricate complex shaped and micro-level vessels such as alveoli using current 3D printing techniques. Therefore, further efforts will be made to print fine scale vascular structures with high resolution. Two-photon polymerization (2PP) is a high-resolution 3D printing process that allows volumetric elements of sub-micrometer resolution to be obtained. Compared to DLP or SLA, the 2PP technique prints structures with a significantly higher spatial resolution, thus fine and complex vascular structures in an artificial organ could be 3D printed. However, compared to other 3D printing techniques, only a few bioinks have been reported with 2PP. Additionally, the size limitation of the object and low printing speed are issues that still need to be resolved. Nevertheless, the 2PP process is expected to be applicable in high-resolution fabrication of vascularized structures.

Furthermore, the application of 4D printing has attracted increasing attention for preparing vascular constructs. Compared to conventional 3D printing techniques, vascular grafts produced by 4D printing could result in enhanced effectiveness and establish higher degree of biomimicry. Blood vessels in human bodies sensitively respond to the change of surrounding environment to hold constancy for maintaining healthy state. By fabricating dynamic 3D biological constructs under external stimulus (i.e. pH, temperature, and light), biomimetic spontaneous deformation, such as blood vessel pulsation that allows blood to flow voluntarily, can be created. Additionally, 4D printed artificial constructs are considered to be beneficial for ex vivo experiments and increased accessibility to ex vivo experiments would reduce unnecessary sacrifice of experimental animals. Although we are still in the early stages of fabricating artificial tissues with vascularized structures, with the rapid development of 3D printing processes, they will soon be available for use in clinical practice.

Declaration of conflicting interests

The author(s) declared no potential conflicts of interest with respect to the research, authorship, and/or publication of this article.

Funding

The author(s) disclosed receipt of the following financial support for the research, authorship, and/or publication of this article: This work was supported by The Catholic University of Korea, Research Fund, 2021 and the National Research Foundation of Korea (NRF) grant funded by the Korea government (MSIT) (2021R1A2C1091301, 2018K1A4A3A01064257, and 2021R1I1A1A01043176), the framework of international cooperation program managed by the National Research Foundation of Korea (2021K2A9A2A06037540), and Korean Fund for Regenerative Medicine funded by Ministry of Science and ICT, and Ministry of Health and Welfare (2021M3E5E5096420, Republic of Korea).

ORCID iDs

Hae-Won Kim https://orcid.org/0000-0001-6400-6100
Hyun-Do Jung https://orcid.org/0000-0001-8632-7431

References

1. Celermajer DS, Chow CK, Marijon E, et al. Cardiovascular disease in the developing world: prevalences, patterns, and

the potential of early disease detection. *J Am Coll Cardiol* 2012; 60: 1207–1216.
2. Flora GD and Nayak MK. A brief review of cardiovascular diseases (atherosclerosis, hypertension, thrombosis and stroke), associated risk factors and current treatment regimes. *Curr Pharm Des* 2019; 25: 4063–4084.
3. Sarkar S, Schmitz-Rixen T, Hamilton G, et al. Achieving the ideal properties for vascular bypass grafts using a tissue engineered approach: a review. *Med Biol Eng Comput* 2007; 45: 327–336.
4. Zhang B, Xu Y, Ma S, et al. Small-diameter polyurethane vascular graft with high strength and excellent compliance. *J Mech Behav Biomed Mater* 2021; 121: 104614.
5. Jang T-S, Lee JH, Kim S, et al. Ta ion implanted nanoridge-platform for enhanced vascular responses. *Biomaterials* 2019; 223 :119461.
6. Park C, Park S, Kim J, et al. Enhanced endothelial cell activity induced by incorporation of nano-thick tantalum layer in artificial vascular grafts. *Appl Surf Sci* 2020; 508: 144801.
7. Park S, Kim J, Lee MK, et al. Fabrication of strong, bioactive vascular grafts with PCL/collagen and PCL/silica bilayers for small-diameter vascular applications. *Mater Des* 2019; 181: 108079.
8. Mi HY, Jiang Y, Jing X, et al. Fabrication of triple-layered vascular grafts composed of silk fibers, polyacrylamide hydrogel, and polyurethane nanofibers with biomimetic mechanical properties. *Mater Sci Eng C* 2019; 98: 241–249.
9. Wu H, He Q, Li L, et al. A facile and versatile superhydrophilic coating on biodegradable PLA stent with stepwise assembly of metal/phenolic networks for mimicking endothelium function. *Chem Eng J* 2022; 427: 130932.
10. Lin M, Firoozi N, Tsai CT, et al. 3D-printed flexible polymer stents for potential applications in inoperable esophageal malignancies. *Acta Biomater* 2019; 83: 119–129.
11. Lee SJ, Jo HH, Lim KS, et al. Heparin coating on 3D printed poly (l-lactic acid) biodegradable cardiovascular stent via mild surface modification approach for coronary artery implantation. *Chem Eng J* 2019; 378: 122116.
12. Jang TS, Cheon KH, Ahn JH, et al. In-vitro blood and vascular compatibility of sirolimus-eluting organic/inorganic hybrid stent coatings. *Colloids Surf B: Biointerfaces* 2019; 179: 405–413.
13. Park S, Lee H, Kim H-E, et al. Bifunctional poly (L-lactic acid)/hydrophobic silica nanocomposite layer coated on magnesium stents for enhancing corrosion resistance and endothelial cell responses. *Mater Sci Eng C* 2021; 127: 112239.
14. Kang M-H, Cheon K-H, Jo KI, et al. An asymmetric surface coating strategy for improved corrosion resistance and vascular compatibility of magnesium alloy stents. *Mater Des* 2020; 196: 109182.
15. Kim S-Y, Han G, Hwang D-B, et al. Design and usability evaluations of a 3D-printed implantable drug delivery device for acute liver failure in preclinical settings. *Adv Healthc Mater* 2021; 10: 2100497.
16. Ahn JH, Kim J, Han G, et al. 3D-printed biodegradable composite scaffolds with significantly enhanced mechanical properties via the combination of binder jetting and capillary rise infiltration process. *Addit Manuf* 2021; 41: 101988.
17. Jain S, Yassin MA, Fuoco T, et al. Engineering 3D degradable, pliable scaffolds toward adipose tissue regeneration; optimized printability, simulations and surface modification. *J Tissue Eng* 2020; 11: 2041731420954316.
18. Jang TS, Kim D, Han G, et al. Powder based additive manufacturing for biomedical application of titanium and its alloys: a review. *Biomed Eng Lett* 2020; 10: 505–516.
19. Chen S, Jang TS, Pan HM, et al. 3D freeform printing of nanocomposite hydrogels through in situ precipitation in reactive viscous fluid. *Int J Bioprinting* 2020; 6: 258.
20. Lee J, Lee H, Cheon KH, et al. Fabrication of poly(lactic acid)/Ti composite scaffolds with enhanced mechanical properties and biocompatibility via fused filament fabrication (FFF)-based 3D printing. *Addit Manuf* 2019; 30: 100883.
21. Jung HD, Jang TS, Lee JE, et al. Enhanced bioactivity of titanium-coated polyetheretherketone implants created by a high-temperature 3D printing process. *Biofabrication* 2019; 11: 045014.
22. Diez-Escudero A, Harlin H, Isaksson P, et al. Porous polylactic acid scaffolds for bone regeneration: a study of additively manufactured triply periodic minimal surfaces and their osteogenic potential. *J Tissue Eng* 2020; 11: 2041731420956541.
23. Jang TS, Jung HD, Pan HM, et al. 3D printing of hydrogel composite systems: recent advances in technology for tissue engineering. *Int J Bioprinting* 2018; 4: 126.
24. Hann SY, Cui H, Esworthy T, et al. Recent advances in 3D printing: vascular network for tissue and organ regeneration. *Transl Res* 2019; 211: 46–63.
25. Chen S, Tan WS, Bin Juhari MA, et al. Freeform 3D printing of soft matters: recent advances in technology for biomedical engineering. *Biomed Eng Lett* 2020; 10: 453–479.
26. Cui H, Nowicki M, Fisher JP, et al. 3D bioprinting for organ regeneration. *Adv Healthc Mater* 2017; 6: 1601118.
27. Patrício SG, Sousa LR, Correia TR, et al. Freeform 3D printing using a continuous viscoelastic supporting matrix. *Biofabrication* 2020; 12: 035017.
28. Nemeno-Guanzon JG, Lee S, Berg JR, et al. Trends in tissue engineering for blood vessels. *J Biomed Biotechnol* 2012; 2012: 956345.
29. Patel B, Wonski BT, Saliganan DM, et al. Decellularized dermis extracellular matrix alloderm mechanically strengthens biological engineered tunica adventitia-based blood vessels. *Sci Rep* 2021; 11(1): 11384.
30. Mozafari H, Zhou C and Gu L. Mechanical contribution of vascular smooth muscle cells in the tunica media of artery. *Nanotechnol Rev* 2019; 8: 50–60.
31. Miri AK, Khalilpour A, Cecen B, et al. Multiscale bioprinting of vascularized models. *Biomaterials* 2019; 198: 204–216.
32. Sällström N, Capel A, Lewis MP, et al. 3D-printable zwitterionic nano-composite hydrogel system for biomedical applications. *J Tissue Eng* 2020; 11: 2041731420967294.
33. Tan WS, Juhari MAB, Shi Q, et al. Development of a new additive manufacturing platform for direct freeform 3D printing of intrinsically curved flexible membranes. *Addit Manuf* 2020; 36: 101563.
34. Wu W, DeConinck A and Lewis JA. Omnidirectional printing of 3D microvascular networks. *Adv Mater* 2011; 23: H178–H183.
35. Grosskopf AK, Truby RL, Kim H, et al. Viscoplastic matrix materials for embedded 3D printing. *ACS Appl Mater Interfaces* 2018; 10: 23353–23361.

36. Chen L, Kenkel SM, Hsieh P-H, et al. Freeform three-dimensionally printed microchannels via surface-initiated photopolymerization combined with sacrificial molding. *ACS Appl Mater Interfaces* 2020; 12: 50105–50112.
37. Costantini M, Colosi C, Święszkowski W, et al. Co-axial wet-spinning in 3D bioprinting: state of the art and future perspective of microfluidic integration. *Biofabrication* 2018; 11: 012001.
38. Molley TG, Jalandhra GK, Nemec SR, et al. Heterotypic tumor models through freeform printing into photostabilized granular microgels. *Biomater Sci* 2021; 9: 4496–4509.
39. Hinton TJ, Jallerat Q, Palchesko RN, et al. Three-dimensional printing of complex biological structures by freeform reversible embedding of suspended hydrogels. *Sci Adv* 2015; 1: e1500758.
40. Gupta P, Lorentz KL, Haskett DG, et al. Bioresorbable silk grafts for small diameter vascular tissue engineering applications: in vitro and in vivo functional analysis. *Acta Biomater* 2020; 105: 146–158.
41. Wang R, Ozsvar J, Aghaei Ghareh Bolagh B, et al. Freestanding hierarchical vascular structures engineered from ice. *Biomaterials* 2019; 192: 334–345.
42. Inoguchi H, Kwon IK, Inoue E, et al. Mechanical responses of a compliant electrospun poly(l-lactide-co-epsilon-caprolactone) small-diameter vascular graft. *Biomaterials* 2006; 27: 1470–1478.
43. Liu H, Zhou H, Lan H, et al. 3D printing of artificial blood vessel: study on multi-parameter optimization design for vascular molding effect in alginate and gelatin. *Micromachines* 2017; 8: 237.
44. Centola M, Rainer A, Spadaccio C, et al. Combining electrospinning and fused deposition modeling for the fabrication of a hybrid vascular graft. *Biofabrication* 2010; 2: 014102.
45. Lee SJ, Kim ME, Nah H, et al. Vascular endothelial growth factor immobilized on mussel-inspired three-dimensional bilayered scaffold for artificial vascular graft application: in vitro and in vivo evaluations. *J Colloid Interface Sci* 2019; 537: 333–344.
46. Wu P, Wang L, Li W, et al. Construction of vascular graft with circumferentially oriented microchannels for improving artery regeneration. *Biomaterials* 2020; 242: 119922.
47. Wang C, Li Z, Zhang L, et al. Long-term results of triple-layered small diameter vascular grafts in sheep carotid arteries. *Med Eng Phys* 2020; 85: 1–6.
48. Sohn SH, Kim TH, Kim TS, et al. Evaluation of 3D templated synthetic vascular graft compared with standard graft in a rat model: potential use as an artificial vascular graft in cardiovascular disease. *Materials* 2021; 14: 1239.
49. Park SJ, Lee J, Choi JW, et al. Additive manufacturing of the core template for the fabrication of an artificial blood vessel: the relationship between the extruded deposition diameter and the filament/nozzle transition ratio. *Mater Sci Eng C* 2021; 118: 111406.
50. Ortega I, Dew L, Kelly AG, et al. Fabrication of biodegradable synthetic perfusable vascular networks via a combination of electrospinning and robocasting. *Biomater Sci* 2015; 3: 592–596.
51. Millik SC, Dostie AM, Karis DG, et al. 3D printed coaxial nozzles for the extrusion of hydrogel tubes toward modeling vascular endothelium. *Biofabrication* 2019; 11: 045009.
52. Zeng Z, Hu C, Liang Q, et al. Coaxial-printed small-diameter polyelectrolyte-based tubes with an electrostatic self-assembly of heparin and YIGSR peptide for antithrombogenicity and endothelialization. *Bioact Mater* 2021; 6: 1628–1638.
53. Zhang Y, Yu Y, Dolati F, et al. Effect of multiwall carbon nanotube reinforcement on coaxially extruded cellular vascular conduits. *Mater Sci Eng C* 2014; 39: 126–133.
54. Cui H, Zhu W, Huang Y, et al. In vitro and in vivo evaluation of 3D bioprinted small-diameter vasculature with smooth muscle and endothelium. *Biofabrication* 2019; 12: 015004.
55. Kesari P, Xu T and Boland T. Layer-by-layer printing of cells and its application to tissue engineering. *Mater Res Soc Symp Proc* 2004; 845: 5–11.
56. Cui X and Boland T. Human microvasculature fabrication using thermal inkjet printing technology. *Biomaterials* 2009; 30: 6221–6227.
57. Nishiyama Y, Nakamura M, Henmi C, et al. Development of a three-dimensional bioprinter: construction of cell supporting structures using Hydrogel and state-Of-the-art Inkjet technology. *J Biomech Eng* 2009; 131: 035001.
58. Xu C, Chai W, Huang Y, et al. Scaffold-free inkjet printing of three-dimensional zigzag cellular tubes. *Biotechnol Bioeng* 2012; 109: 3152–3160.
59. Christensen K, Xu C, Chai W, et al. Freeform inkjet printing of cellular structures with bifurcations. *Biotechnol Bioeng* 2015; 112: 1047–1055.
60. Melchiorri AJ, Hibino N, Best CA, et al. 3D-printed biodegradable polymeric vascular grafts. *Adv Healthc Mater* 2016; 5(3): 319–325.
61. Bracaglia LG, Messina M, Winston S, et al. 3D printed pericardium hydrogels to promote wound healing in vascular applications. *Biomacromolecules* 2017; 18: 3802–3811.
62. Chiu YC, Shen YF, Lee AK, et al. 3D printing of amino resin-based photosensitive materials on multi-parameter optimization design for vascular engineering applications. *Polymers* 2019; 11: 1394.
63. L'Heureux N, Dusserre N, Konig G, et al. Human tissue-engineered blood vessels for adult arterial revascularization. *Nat Med* 2006; 12(3): 361–365.
64. Syedain ZH, Meier LA, Bjork JW, et al. Implantable arterial grafts from human fibroblasts and fibrin using a multi-graft pulsed flow-stretch bioreactor with noninvasive strength monitoring. *Biomaterials* 2011; 32: 714–722.
65. Zhao J, Liu L, Wei J, et al. A novel strategy to engineer small-diameter vascular grafts from marrow-derived mesenchymal stem cells. *Artif Organs* 2012; 36: 93–101.
66. Nakayama Y, Furukoshi M, Terazawa T, et al. Development of long in vivo tissue-engineered "Biotube" vascular grafts. *Biomaterials* 2018; 185: 232–239.
67. Nakayama Y, Kaneko Y, Okumura N, et al. Initial 3-year results of first human use of an in-body tissue-engineered autologous "Biotube" vascular graft for hemodialysis. *J Vasc Access* 2020; 21: 110–115.
68. Itoh M, Nakayama K, Noguchi R, et al. Correction: scaffold-free tubular tissues created by a bio-3D printer undergo remodeling and endothelialization when implanted in rat aortae. *PLoS One* 2015; 10: e0145971.
69. Zhou Y, Gui Q, Yu W, et al. Interfacial diffusion printing: an efficient manufacturing technique for artificial tubular grafts. *ACS Biomater Sci Eng* 2019; 5(11): 6311–6318.

70. Zheng F, Derby B and Wong J. Fabrication of microvascular constructs using high resolution electrohydrodynamic inkjet printing. *Biofabrication* 2021; 13: 035006.
71. Cheng B, Xing YM, Shih NC, et al. The formulation and characterization of 3D printed grafts as vascular access for potential use in hemodialysis. *RSC Adv* 2018; 8: 15471–15479.
72. Molley TG, Jalandhra GK, Nemec SR, et al. Freeform printing of heterotypic tumor models within cell-laden microgel matrices. *bioRxiv*, 2020.
73. Compaan AM, Song K, Chai W, et al. Cross-linkable microgel composite matrix bath for embedded bioprinting of perfusable tissue constructs and sculpting of solid objects. *ACS Appl Mater Interfaces* 2020; 12(7): 7855–7868.
74. Štumberger G and Vihar B. Freeform perfusable microfluidics embedded in hydrogel matrices. *Materials* 2018; 11: 2529.
75. Bhattacharjee T, Zehnder SM, Rowe KG, et al. Writing in the granular gel medium. *Sci Adv* 2015; 1: e1500655.
76. Savoji H, Davenport Huyer L, Mohammadi MH, et al. 3D printing of vascular tubes using bioelastomer prepolymers by freeform reversible embedding. *ACS Biomater Sci Eng* 2020; 6: 1333–1343.
77. Noor N, Shapira A, Edri R, et al. 3D printing of personalized thick and perfusable cardiac patches and hearts. *Adv Sci* 2019; 6: 1900344.
78. Lee S, Sani ES, Spencer AR, et al. Human-recombinant-elastin-based bioinks for 3D bioprinting of vascularized soft tissues. *Adv Mater* 2020; 32: e2003915.
79. Afghah F, Altunbek M, Dikyol C, et al. Preparation and characterization of nanoclay-hydrogel composite support-bath for bioprinting of complex structures. *Sci Rep* 2020; 10: 5257.
80. Norotte C, Marga FS, Niklason LE, et al. Scaffold-free vascular tissue engineering using bioprinting. *Biomaterials* 2009; 30: 5910–5917.
81. Skylar-Scott MA, Huang JY, Lu A, et al. An orthogonal differentiation platform for genomically programming stem cells, organoids, and bioprinted tissues. *bioRxiv*, 2020.
82. Skylar-Scott MA, Uzel SGM, Nam LL, et al. Biomanufacturing of organ-specific tissues with high cellular density and embedded vascular channels. *Sci Adv* 2019; 5: eaaw2459.
83. Applegate MB, Coburn J, Partlow BP, et al. Laser-based three-dimensional multiscale micropatterning of biocompatible hydrogels for customized tissue engineering scaffolds. *Proc Natl Acad Sci* 2015; 112: 12052–12057.
84. Brandenberg N and Lutolf MP. In situ patterning of microfluidic networks in 3D cell-laden hydrogels. *Adv Mater* 2016; 28: 7450–7456.
85. Arakawa CK, Badeau BA, Zheng Y, et al. Multicellular vascularized engineered tissues through user-programmable biomaterial photodegradation. *Adv Mater* 2017; 29: 1703156.
86. Zhu W, Qu X, Zhu J, et al. Direct 3D bioprinting of prevascularized tissue constructs with complex microarchitecture. *Biomaterials* 2017; 124: 106–115.
87. Grigoryan B, Paulsen SJ, Corbett DC, et al. Multivascular networks and functional intravascular topologies within biocompatible hydrogels. *Science* 2019; 364: 458–464.
88. Thomas A, Orellano I, Lam T, et al. Vascular bioprinting with enzymatically degradable bioinks via multi-material projection-based stereolithography. *Acta Biomater* 2020; 117: 121–132.
89. Annabi N, Zhang Y-N, Assmann A, et al. Engineering a highly elastic human protein-based sealant for surgical applications. *Sci Transl Med* 2017; 9: eaai7466.
90. Friedrich LM and Seppala JE. Simulated filament shapes in embedded 3D printing. *Soft Matter* 2021; 17: 8027–8046.
91. Tokpavi DL, Magnin A and Jay P. Very slow flow of Bingham viscoplastic fluid around a circular cylinder. *J Non-Newton Fluid Mech* 2008; 154: 65–76.
92. Mitsoulis E. Flows of viscoplastic materials: models and computations. *Rheol Rev* 2007; 2007: 135–178.
93. Uchida T and Onoe H. 4D printing of multi-hydrogels using direct ink writing in a supporting viscous liquid. *Micromachines* 2019; 10: 433.
94. Jin Y, Song K, Gellermann N, et al. Printing of hydrophobic materials in fumed silica nanoparticle suspension. *ACS Appl Mater Interfaces* 2019; 11: 29207–29217.
95. O'Bryan CS, Bhattacharjee T, Niemi SR, et al. Three-dimensional printing with sacrificial materials for soft matter manufacturing. *MRS Bull* 2017; 42: 571–577.
96. Rodriguez MJ, Dixon TA, Cohen E, et al. 3D freeform printing of silk fibroin. *Acta Biomater* 2018; 71: 379–387.
97. O'Bryan CS, Bhattacharjee T, Marshall SL, et al. Commercially available microgels for 3D bioprinting. *Bioprinting* 2018; 11: e00037.
98. Jiménez Torres JA, Peery SL, Sung KE, et al. LumeNEXT: a practical method to pattern luminal structures in ECM gels. *Adv Healthc Mater* 2016; 5: 198–204.
99. He R, Yunus D, Uhl C, et al. Fabrication of circular microfluidic channels through grayscale dual-projection lithography. *Microfluid Nanofluidics* 2017; 21: 13.
100. Padera TP, Stoll BR, Tooredman JB, et al. Cancer cells compress intratumour vessels. *Nature* 2004; 427: 695–695.
101. Goel S, Duda DG, Xu L, et al. Normalization of the vasculature for treatment of cancer and other diseases. *Physiol Rev* 2011; 91: 1071–1121.
102. Xie R, Zheng W, Guan L, et al. Engineering of hydrogel materials with perfusable microchannels for building vascularized tissues. *Small* 2020; 16: e1902838.
103. Chen C, Mehl BT, Munshi AS, et al. 3D-printed microfluidic devices: fabrication, advantages and limitations – a mini review. *Anal Methods* 2016; 8: 6005–6012.
104. Han WT, Jang T, Chen S, et al. Improved cell viability for large-scale biofabrication with photo-crosslinkable hydrogel systems through a dual-photoinitiator approach. *Biomater Sci* 2020; 8: 450–461.
105. Lee J, Oh SJ, An SH, et al. Machine learning-based design strategy for 3D printable bioink: elastic modulus and yield stress determine printability. *Biofabrication* 2020; 12: 035018.
106. Ruberu K, Senadeera M, Rana S, et al. Coupling machine learning with 3D bioprinting to fast track optimisation of extrusion printing. *Appl Mater Today* 2021; 22: 100914.